ELSEVIER

Coordination Chemistry Reviews
182 (1999) 373–410

COORDINATION CHEMISTRY REVIEWS

Mechanistic studies in coordination chemistry

Rudi van Eldik *

Institute for Inorganic Chemistry, University of Erlangen-Nürnberg, Egerlandstr. 1, 91058 Erlangen, Germany

Received 24 March 1998; received in revised form 27 July 1998

Contents

Abstract . . . 373
1. Introduction . . . 374
2. Ligand substitution reactions . . . 375
   2.1. Labilization by a hydroxo ligand . . . 376
   2.2. Labilization by a metal–carbon bond . . . 378
   2.3. Labilization by chelate effects . . . 379
   2.4. Indirect mechanistic information . . . 381
3. Activation of small molecules . . . 382
   3.1. Activation of dioxygen . . . 383
   3.2. Activation of carbon monoxide . . . 387
   3.3. Activation of carbon dioxide . . . 390
   3.4. Activation of sulfur dioxide . . . 393
   3.5. Activation of nitrogen oxides . . . 397
4. Electron transfer reactions . . . 398
5. Final remarks . . . 407
Acknowledgements . . . 407
References . . . 407

Abstract

The elucidation of the mechanisms of thermal reactions in inorganic, organometallic, bioinorganic and environmental systems through the application of modern kinetic techniques is described. The processes studied include ligand substitution, activation of small molecules, and electron transfer reactions. Detailed mechanistic insight was obtained through the application of rapid-scan and high pressure kinetic techniques, as well as from theoretical

* Fax: +49-9131-8527387; e-mail: vaneldik@anorganik.chemie.uni-erlangen.de.

PII: S0010-8545(98)00213-6

calculations and modelling of suggested mechanisms.

Keywords: Reaction mechanism; Volume profile; Ligand substitution; Small molecule activation; Homogeneous catalysis; Electron transfer; Redox cycling

1. Introduction

A special issue of Coordination Chemistry Reviews dedicated to German chemistry provides the welcome opportunity to review the accomplishments achieved in mechanistic studies in coordination chemistry that has been the focus of many investigations performed by our group over the past two decades. Mechanistic studies in coordination chemistry do not have an extended tradition in German chemistry. As the other contributions in this special issue will clearly demonstrate, German inorganic chemistry has a much stronger synthetic and structural oriented tradition. Although many inorganic chemists are interested also in the reactivity of the newly synthesized complexes, few actually study the details of the underlying reaction mechanisms.

To some extent we are outsiders to the typical field of German coordination chemistry. We have focused our attention on systems that involve reactions of inorganic, organometallic and bioinorganic complexes, as well as those that involve reactions of general atmospheric and environmental interest. Much of our work has involved the application of high pressure kinetic and thermodynamic techniques in order to construct volume profiles for inorganic reactions. This aspect, however, will not only be treated in this review, since reports on this topic have appeared elsewhere [1–9]. In addition, we want to focus on some of our mechanistic studies in coordination chemistry that were performed at ambient pressure only, especially those in which detailed insight was gained through the application of rapid-scan techniques at ambient and low temperatures, and those in which a theoretical approach was adopted.

It has been our philosophy in the past to obtain as much as possible mechanistic insight from detailed kinetic investigations as a function of as many as possible experimental variables. These include the concentrations of the reactants and products, the composition of the solvent, pH, buffer composition, and ionic strength, which all form part of the chemical variables in mechanistic studies. In addition, there are two physical variables available in such studies, viz. temperature and pressure, and we have made use of both of these where possible. Such detailed kinetic data can provide along with all other known chemical and structural properties of the system and possible intermediates, detailed insight into the nature of the underlying reaction mechanism. In many cases our insight is restricted by the number of variables covered during such investigations. The suggested mechanism based on this information will only then approach the real mechanism when it is in line with all available experimental as well as theoretical data.

In this contribution we will review our accomplishments in different areas of inorganic, organometallic, bioinorganic and atmospheric chemistry, by treating different types of reactions. In this treatment we will restrict ourselves to thermal reactions, including some that are induced via flash photolysis and pulse radiolysis. A detailed treatment on mechanistic studies from our group dealing with photochemical reactions can be found elsewhere [7,8]. We will start with ligand substitution processes, then move to the activation of small molecules, which in many cases is preceded by a ligand substitution process, and finally come to electron transfer reactions, which again in many cases is an essential part of the activation of small molecules. This rather superficial categorization of the presentation does enable a systematic treatment of our accomplishments, as well as a systematic development of basic principles and insights gained for the non-informed reader.

2. Ligand substitution reactions

The general understanding of ligand substitution mechanisms of square planar and octahedral complexes since the earlier concepts were developed [10,11], benefited greatly from the numerous high pressure kinetic studies performed in this area especially within Europe over the past two decades. In this respect it has especially been the group of André Merbach in Lausanne that have contributed in an impressive way to resolve the mechanisms of symmetrical solvent and ligand exchange processes on transition metal complexes [4,5,12–14]. Solvent exchange processes are the most fundamental substitution reactions that characterize the lability and reaction mechanism of a metal center within a coordination geometry. For these reactions the interpretation of the volume of activation becomes rather straight forward since these reactions do not involve major changes in solvation due to changes in dipole moments and electrostriction, which can in the case of non-symmetrical reactions complicate the interpretation significantly. The results and mechanistic information obtained from these studies are presently well accepted by the mechanistic community, but have in the past resulted in several discrepancies in the literature, especially with theoretical chemists.

The activation volumes for solvent exchange on the divalent cations of the first row of transition metals exhibit clear evidence for a mechanistic changeover along the series, i.e. from more associative for the earlier, larger cations to a more dissociative one for the later, smaller cations [4,5]. It has been claimed on the basis of theoretical calculations [15–18] that the interpretation of such activation volume data could be considered faulty, and arguments were presented against a mechanistic changeover along the series. Additional theoretical calculations were needed in order to investigate the validity of the mechanistic proposals that were based on calculations, in an effort to resolve the disparate conclusions.

The original studies [15–18] involved ab initio self consistent field (SCF) calculations of the binding energies, ligand-field effects, water exchange reactions, and exchange of hexahydrated divalent first row transition metal cations. In subsequent work, Rotzinger [19,20] succeeded in computing the structures of the transition

states and the intermediates formed during the water exchange reactions of the first row transition metals with ab initio methods at the Hartree-Fock or complete active space-SCF (CAS-SCF) level. It was now possible to generate A, I_a, I_d and D pathways, and to optimize the structures of the transition and intermediate states. Furthermore, the calculated bond length changes that occurred during the activation process were entirely consistent with the activation volume data, and indicated that an associative interchange mechanism can operate for some metal ions, in contrast to the previous theoretical prediction [18].

Density functional theory has also been applied successfully to describe the solvent exchange mechanism for aquated Pd(II), Pt(II) and Zn(II) cations [21,22]. Our own work on aquated Zn(II) [22] was stimulated by our interest in the catalytic activity of such metal ions and by the absence of any solvent (water) exchange data for this cation. The optimized transition state structure shown in Fig. 1 clearly demonstrates the dissociative nature of the process; in no way could a seventh water molecule be forced to enter the coordination sphere without the simultaneous dissociation of one of the six coordinated water molecules.

2.1. Labilization by a hydroxo ligand

The mechanistic understanding of solvent exchange reactions has reached the point where specific labilization effects can be studied in a systematic way. In this respect it is appropriate to refer to the significant *trans*-labilization caused by the deprotonation of a coordinated water molecule. In the case of hexaaqua complexes of Fe(III), Rh(III) and Ir(III), such deprotonation can cause an increase in the water exchange rate of between 700 and 20000 times at 298 K [23]. This labilization is also accompanied by a changeover in mechanism from a more associative interchange for the hexaaqua complex ions to a more dissociative interchange mechanism for the pentaaquamonohydroxo complex ions. As a result of rapid proton exchange, labilization by coordinated hydroxide is not site specific, with the result that all five coordinated water molecules are labilized to the same extent.

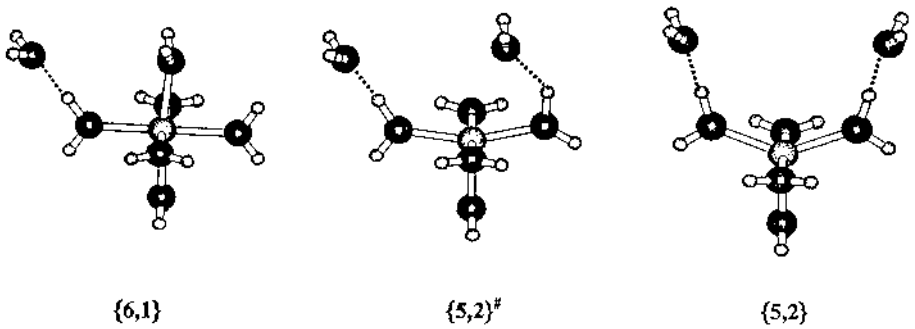

Fig. 1. Optimized structures for the reactant {6,1}, transition state $\{5,2\}^{\#}$ and intermediate complex {5,2} obtained for solvent exchange on $Zn(H_2O)_6^{2+}$ [22].

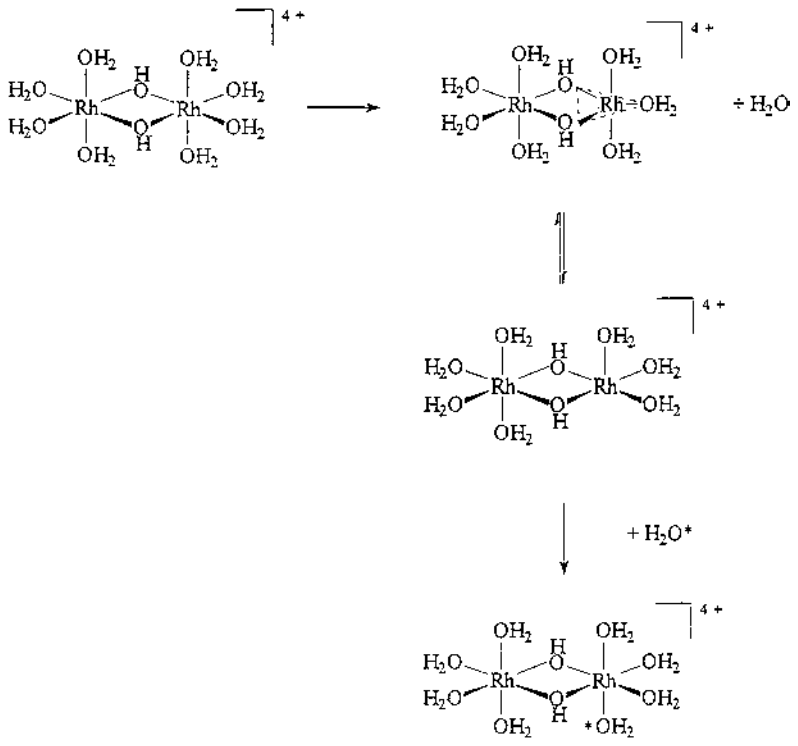

Fig. 2. Suggested Berry pseudo-rotation mechanism to account for the similarity in the exchange rate constants of the *cis* and *trans* coordinated water molecules in the dihydroxo bridged Rh(III) dimer [24].

We studied recently the effect of pressure on the water exchange reaction of the dihydroxo bridged Rh(III) dimer in which the hydroxo labilization must now be site specific [24]. ^{17}O-NMR experiments clearly demonstrated that the coordinated water molecules located *cis* and *trans* to the hydroxo bridging ligands exhibit different chemical shifts, and exchange significantly faster with the bulk solvent than the bridging hydroxo groups. Surprisingly, however, was the finding that these water molecules exchange at a rather similar rate (ca. 5×10^{-7} s^{-1} at 298 K), which is ca. 10^2 faster than the water exchange on the hexaaquarhodium(III) monomer, but ca. 10^2 slower than the exchange on the pentaaquamonohydroxo monomer. The estimated volumes of activation were found to be between $+9$ and $+10$ cm^3 mol^{-1}, which is a clear indication for a dissociative exchange mechanism. The surprising similarity in the exchange rates of the *cis* and *trans* water molecules becomes quite understandable in terms of a dissociative mechanism. Dissociation of the more labile *trans* water molecules will result in the formation of a trigonal bipyramidal five-coordinate intermediate, which can via a Berry pseudo-rotation convert to a tetragonal pyramidal species, with the consequence that the entering solvent molecule will take the *cis* position as presented schematically in Fig. 2. Thus, dissociative solvent exchange in such complexes results in an almost equal labilization of both the *cis* and *trans* bound water molecules.

2.2. Labilization by a metal–carbon bond

Other examples of large labilization effects include the introduction of metal–carbon bonds on traditionally inert metal centers such as Co(III), Rh(III) and Ir(III). For instance, the presence of Cp* in the complexes $M(Cp^*)(H_2O)_3^{2+}$ (M = Rh(III) and Ir(III)) causes an increase in the solvent exchange rate constant of 10^{14} as compared with the hexaaqua species [25]. The volumes of activation support the operation of a dissociative interchange mechanism in both cases. In the case of the $Co(NH_3)_5CH_3^{2+}$ complex, the strong *trans* labilization caused by the metal–carbon bond does not only show up in the ground state structure [26], but also causes this complex to become extremely labile and the substitution reaction is characterized by a very positive volume of activation, suggesting a limiting dissociative mechanism [27]. The introduction of carbon bonded alkanes on rhodoximes causes a drastic increase in the lability of the *trans* position. The nature of the organic ligand not only controls the rate of the substitution process, but also the nature of the mechanism. Based on the reported volumes of activation [28], it could be concluded that CH_3 induces a fast substitution process that follows a dissociative interchange mechanism, whereas for the weaker CH_2CF_3 donor group, the substitution reaction is significantly slower and follows an associative interchange mechanism. A typical volume profile constructed for the reversible binding of iodide in the case of the methyl complex is shown in Fig. 3. Interesting enough, whether the organic group was varied or not for a given nucleophile, all reactions studied were characterized by moderately negative entropies of activation. Thus, the additional potential mechanistic discrimination power of the pressure variable has been aptly exploited in *trans*-rhodoxime substitution behaviour.

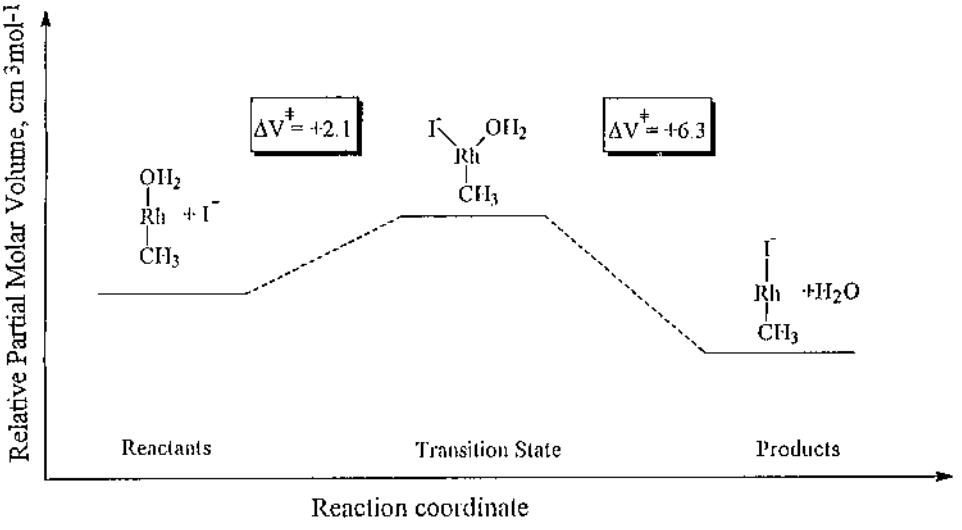

Fig. 3. Volume profile for the nucleophilic substitution of *trans*-$Rh^{III}(dmg)_2(CH_3)(H_2O)$ by iodide [28].

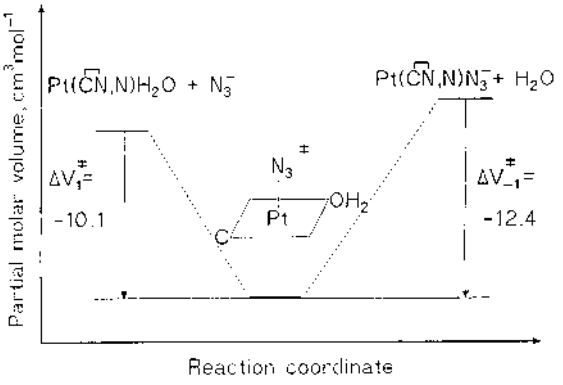

Fig. 4. Volume profile for anation of $Pt^{II}(C-N,N)H_2O^+$ by azide [29].

The introduction of metal–carbon bonds in square-planar complexes has also resulted in significant labilization effects. The basic question dealt with, was the possibility to find evidence for a changeover in the substitution mechanism of such systems. In general d^8 systems follow an associative substitution mechanism, but specific labilization effects may induce a dissociative substitution mode. The introduction of a single metal–carbon bond in complexes of the type $Pt(C-N,N)H_2O^+$ and $Pt(N-C-N)H_2O^+$ [29,30], where C–N and N–C–N represent $C_6H_4(CH_2NMe_2)$ and $C_6H_3(CH_2NMe_2)_2$, respectively, caused an increase in lability of the coordinated water molecule by a factor of 10^4 in comparison with a diethylenetriamine complex of the type $Pt(N-N-N)H_2O^{2+}$. However, the activation volumes indicated clearly that the substitution reactions still follow an associative mechanism. A typical volume profile for one of the systems is reported in Fig. 4. The increase in lability in these complexes was accounted for in terms of an increase in the electrophilicity of the metal center due to back bonding effects with the in plane benzyl chelate. It is clear from a comparison with other literature data [31,32] that more than one metal–carbon bond is required in order to cause a changeover to a dissociative substitution mode.

2.3. Labilization by chelate effects

Solvent exchange and ligand substitution reactions can be drastically affected by the influence of chelating ligands. For instance, solvent exchange on $Fe(H_2O)_6^{3+}$ occurs at a rate of 2×10^2 s^{-1} at 298 K and is characterized by an activation volume of -5.4 cm^3 mol^{-1}, typical for an associative interchange mechanism [33]. Introduction of hexadentate chelating ligands such as ethylenediaminetetraacetate, cyclohexyldiaminetetraacetate and phenylenediaminetetraacetate to produce seven-coordinate complexes of the type $Fe^{III}(L)H_2O^-$, result in solvent exchange rates of ca. 10^7 s^{-1} at 298 K (i.e. an acceleration of 10^5) and volumes of activation of between $+3.2$ and $+4.6$ cm^3 mol^{-1}, which are typical for a dissociative interchange process [34,35]. Thus the increase in lability is once again accompanied by a changeover in the nature of the ligand substitution mechanism.

In the case of substitution reactions on Ru(III), the lability of the hexaaqua complex can be increased by up to six orders of magnitude by introducing a chelating ligand such as ethylenediaminetetraacetate (EDTA) into the coordination sphere [36,37]. The resulting $Ru^{III}(EDTA)H_2O^-$ complex is a six-coordinate species in which EDTA is bound in a pentadentate way. The displacement of the coordinated water molecule is characterized by a bell-shaped pH dependence for which either protonation of the non-coordinated carboxylate arm of edta or deprotonation of the coordinated water molecule leads to an almost complete suppression of the lability of the $Ru(EDTA)H_2O^-$ species. The activation parameters (especially the $\Delta V^{\#}$ values) support strongly the operation of a limiting associative substitution mechanism for the labile $Ru(EDTA)H_2O^-$ complex. This increase in reactivity and the associative substitution mechanism were suggested to be due to distortion of the metal–ligand bonds and labilization of the coordinated water molecule arising from H-bonding with the free carboxylate moiety [36,37].

The introduction of a multidentate ligand into the coordination sphere of an aquated metal ion can also cause a change in coordination geometry accompanied by a drastic decrease in lability. One such example we have dealt with involved ligand substitution reactions on Cu(II). The extremely rapid dissociative solvent exchange on $Cu(H_2O)_6^{2+}$ [38] is slowed down by three orders of magnitude for the trigonal bipyramidal $Cu(tren)H_2O^{2+}$ ion. Water exchange and complex-formation reactions of the tren complex proceed by an associative interchange mechanism as evidenced by significantly negative volumes of activation, viz. -4.7 cm^3 mol^{-1} for water exchange and between -7.5 and -10 cm^3 mol^{-1} for ligand substitution, respectively [39]. Some typical volume profiles for such ligand substitution reactions are shown in Fig. 5, from which the compact nature of the transition state can be seen. Modifications of the tren ligand drastically affect the coordination geometry as well as the lability of the complexes [40].

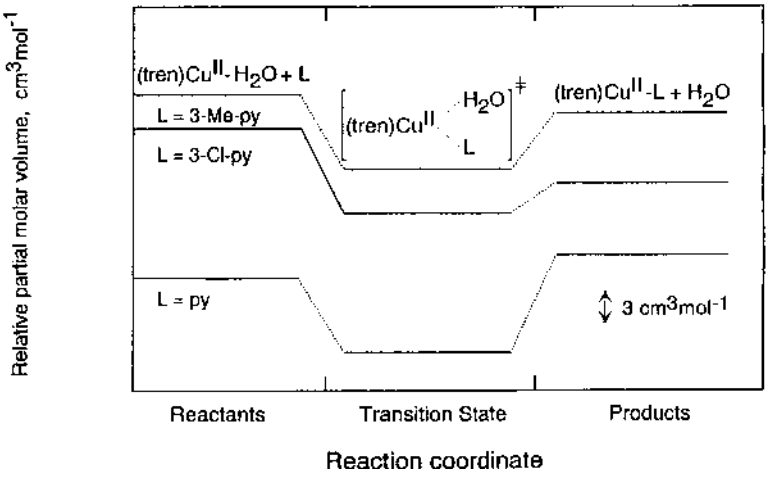

Fig. 5. Volume profiles for complex-formation reactions of $Cu(tren)H_2O^{2+}$ by a series of pyridine ligands [39].

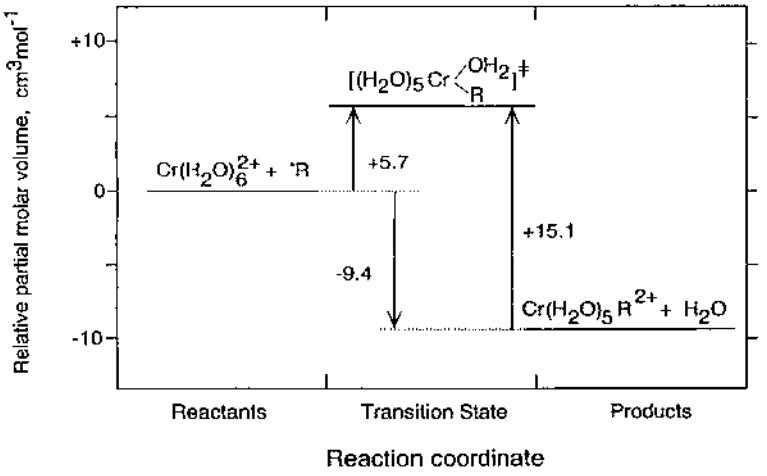

Fig. 6. Volume profile for the reaction of an aliphatic radical with $Cr(H_2O)_6^{2+}$ [42].

2.4. Indirect mechanistic information

In some cases the investigated reaction can indirectly reveal mechanistic information on ligand substitution processes that form an integral part of the studied reaction. For instance during the formation and cleavage of metal–carbon σ bonds, ligand substitution plays an important role. The application of pulse radiolysis techniques demonstrated that the reaction of the methyl radical with $Co^{II}(nta)(H_2O)_2^-$ to produce $Co^{III}(nta)(CH_3)(H_2O)^-$ is characterized by a volume of activation of $+6\ cm^3\ mol^{-1}$ and an overall reaction volume of $-16\ cm^3\ mol^{-1}$ [41]. This indicates clearly that the transition state has a significantly higher partial molar volume than either the reactant or product states, and that the binding of the methyl radical is controlled by solvent exchange on $Co^{II}(nta)(H_2O)_2^-$, which follows a dissociative interchange mechanism. The large volume collapse following the transition state was ascribed to metal–carbon bond formation which is accompanied by oxidation of Co(II) to Co(III).

A similar result was found for the reaction of aquated Cr(II) with ten different aliphatic radicals (R) to produce $Cr^{III}(H_2O)_5R^{2+}$ [42]. The observed second order rate constants were all very similar for these reactions and agreed remarkably well with the solvent exchange rate constant of $Cr(H_2O)_6^{2+}$. Furthermore, the volumes of activation all varied between $+3.4$ and $+6.3\ cm^3\ mol^{-1}$, from which it was concluded that water exchange on aquated Cr(II) controlled the formation of $Cr–R^{2+}$, and that water exchange occurs according to an I_d mechanism. A typical volume profile for this reaction is reported in Fig. 6. These and other studies on the interaction of metal complexes with free radicals suggest that for non-diffusion controlled processes, the radicals can be treated as normal nucleophiles in ligand substitution processes, which are often controlled by solvent exchange on the metal complex [43].

A final example concerns the question to what extent a multiple series of ligand substitution reactions can lead to the irreversible exchange of two metal centers. The system that we investigated involves the exchange of Mn and Cr in the following series of reactions [44]:

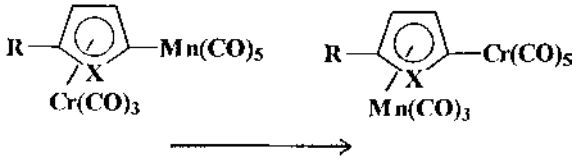

1 X=S, R=H
2 X=S, R=Me
3 X=Se, R=H

4 X=S, R=H
5 X=S, R=Me
6 X=Se, R=H

The kinetics of such metal exchange reactions can be followed using a variety of spectroscopic techniques. A detailed kinetic study indicated that the reactions: follow first order behaviour; do not exhibit a meaningful dependence on the polarity of the solvent; are independent of the concentration of the complex; do not undergo exchange with ^{13}CO during the metal exchange procees; and exhibit activation entropies and activation volumes close to zero. All these observations underline the operation of an intramolecular metal exchange process, for which the suggested mechanism can be presented as follows:

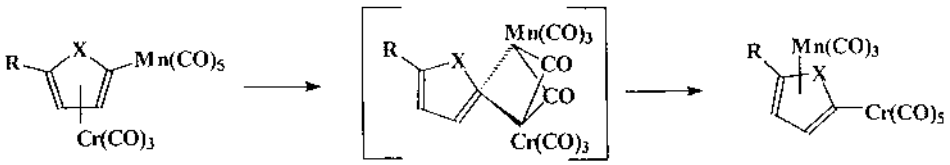

1 X=S, R=H
2 X=S, R=Me
3 X=Se, R=H

4 X=S, R=H
5 X=S, R=Me
6 X=Se, R=H

3. Activation of small molecules

In this section we will address the coordination chemistry of a wide variety of systems that all, in a direct or indirect way, involve the activation of small molecules. The treated systems are of biological, environmental or industrial interest, and form the basis of homogeneously catalyzed processes.

3.1. Activation of dioxygen

Excellent reviews on the activation of dioxygen by transition metal complexes have appeared recently [45–48]. In some cases the details of the underlying reaction mechanisms could be resolved from kinetic studies, usually involving rapid kinetic techniques and low temperature experiments in order to detect possible reaction intermediates [48]. In many cases, however, detailed insight was not available, and some of the given examples will demonstrate how our efforts were devoted to fulfil this need.

One of the most fundamental questions when dealing with the activation of dioxygen by transition metal complexes is the way in which these species really interact with each other. Are these processes controlled kinetically by substitution or by electron transfer reactions? In collaboration with the group of J.H. Espenson (Ames, Iowa) we studied a model system that involved the binding of dioxygen to a macrocyclic hexamethylcyclam Co(II) complex to form the corresponding Co(III) superoxo species [49], thus modelling the first redox activation step of dioxygen. The overall reaction thus involves ligand substitution and electron transfer, the question being which occurs first. From the pressure dependence of the overall equilibrium a reaction volume of $-22\ cm^3\ mol^{-1}$ was determined, which demonstrates that the displacement of a water molecule on the Co(II) complex by dioxygen is accompanied by a significant volume collapse, probably mainly due to the oxidation of Co(II) to Co(III) during the overall reaction. The kinetics of the reaction could be studied by flash-photolysis, since the dioxygen complex can be photo-dissociated by irradiation into the CT band, and the subsequent re-equilibration could be followed on the microsecond time scale. From the effect of pressure on the binding and release of dioxygen, the activation volumes for both processes could be determined. A combination of these activation volumes resulted in a reaction volume that is in excellent agreement with the value determined directly from the equilibrium measurements as a function of pressure. The volume profile for this reaction is given in Fig. 7. The small volume of activation associated with the binding of dioxygen is clear evidence for a rate-limiting interchange of ligands, dioxygen for water, which is followed by an intramolecular electron transfer reaction between Co(II) and O_2 to form $Co^{III}–O_2^-$, the superoxo species. It is the latter process that accounts for the large volume reduction en route to the reaction products. Thus, during flash-photolysis, electron transfer in the reverse direction occurs due to irradiation into the CT band, which is followed by the rapid release of dioxygen. Thus, our volume profile analysis has resolved the question concerning the nature of the rate-determining step during the activation of dioxygen by this model macrocyclic Co(II) complex [49].

Following earlier work on the binding of dioxygen to myoglobin [50,51], we more recently generated a volume profile for the binding of dioxygen to hemerythrin [52]. The $\Delta V^{\#}$ values for the on and off reactions as well as the overall reaction volume are ca. twice the magnitudes of those for the corresponding myoglobin case. In the hemerythrin system two Fe(II) centers are oxidized to Fe(III) during which dioxygen is reduced and bound as hydroperoxide to one Fe(III) center. The $\Delta V^{\#}_{on}$ value

can partly be accounted for in terms of desolvation of oxygen during its entrance into the protein. The value is, however, such that it suggests some form of dynamic breathing motion of the protein that momentarily causes an opening up of a cleft and enables oxygen to enter the protein. The significant volume decrease that occurs following the formation of the transition state can be ascribed to the oxidation of the Fe centres and the reduction of O_2 to O_2^{2-}. The fact that the overall volume collapse is almost double that observed for the oxygenation of myoglobin may indicate similar structural features in oxyhemerythrin and oxymyoglobin. This would suggest that a description of the bonding mode as $Fe^{III}–O_2^-$ or $Fe^{III}–O_2H$ (H from histidine E7) instead of $Fe^{II}–O_2$, may be more appropriate for oxymyoglobin.

A suitable model for the oxygen carrier protein hemerythrin is $[Fe_2$(Et-HPTB)(OBz)$](BF_4)_2$, Et-HPTB = *N*,*N*,*N*′,*N*′-tetrakis[(*N*-ethyl-2-benzimidazolyl)-methyl]-2-hydroxy-1,3-diaminopropane, OBz = benzoate; it can mimic the formation of a binuclear peroxo iron complex in the natural system [53]. In this case it was possible to follow the irreversible uptake of dioxygen. The measured value of -12.8 cm^3 mol^{-1} for the activation volume of the reaction together with the negative value of the activation entropy, confirm the highly structured nature of the transition state.

Oxidation reactions of chelated Fe(II) complexes are all accelerated markedly by pressure and accompanied by negative volumes of activation [54]. These can be ascribed to the binding of dioxygen that is accompanied by the oxidation of Fe(II) to Fe(III) and the reduction of dioxygen to superoxide and peroxide, processes that are all expected to lead to a decrease in partial molar volume. In a recent reinvestigation of the Fe^{II}(EDTA) oxidation reaction [55] it was possible to resolve the different reaction steps that form part of the oxidation process, and to interpret the negative volumes of activation in a more detailed way. Depending on the nature

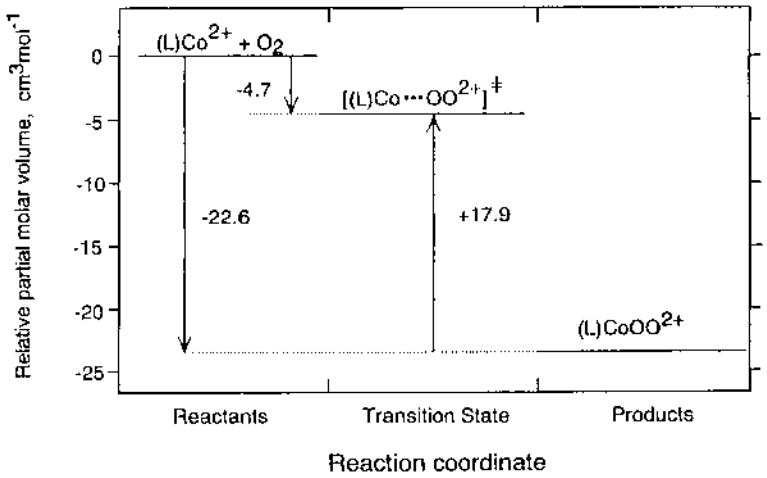

Fig. 7. Volume profile for the reaction of dioxygen with the hexamethylcyclam complex of Co(II) [49].

of the polyaminecarboxylate chelate, up to four kinetically distinguishable steps could be observed in the presence of an excess of the Fe(II) complex [55,56]. These involved coordination of dioxygen, intramolecular electron transfer to produce the Fe(III) superoxo complex, subsequent substitution by a second Fe(II) species to produce a mixed valence superoxo-bridged complex, followed by intramolecular electron transfer to form a peroxo-bridged binuclear Fe(III) complex, which rapidly decomposed in acidic medium to produce the monomeric Fe(III) complex and hydrogen peroxide.

Tyrosinase, a dinuclear copper protein, is a monoxygenase which activates dioxygen for the ortho hydroxylation of monophenols. Efforts to model this protein functionally led to the development of a series of dinuclear copper model complexes [48,57]. Very detailed and sophisticated kinetic measurements have established that during the reaction of a series of dinuclear copper(I) complexes with dioxygen, intramolecular ligand hydroxylation occurs leading to phenolate bridged copper(II) complexes [48]. We performed a study of the reaction of $[Cu_2(mac)(CH_3CN)_2](PF_6)_2$ (mac = 3,6,9,17,20,23-hexatricyclo[23.3.1.1]tiaconta1-(29),2,9,11(30),-12(13),14,16,23,-25,27-decaene) with dioxygen [57]. The activation parameters were found to be $\Delta H^{\#} = 32 \pm 2$ kJ mol^{-1}, $\Delta S^{\#} = -146 \pm 8$ J K^{-1} mol^{-1} and $\Delta V^{\#} = -21 \pm 1$ cm^3 mol^{-1}. In a rate determining step a peroxo complex is formed as an intermediate, which then reacts in a very fast reaction to give the final product. The negative $\Delta S^{\#}$ and $\Delta V^{\#}$ values support the idea of a highly structured transition state that is formed as a result of the presence of the highly reactive and easily oxidizable cuprous species. The negative volume of activation is a strong indication of Cu–O_2 bond formation that is accompanied by electron transfer to produce the Cu(II)–O_2–Cu(II) peroxo intermediate. The formal oxidation of Cu(I) to Cu(II) and reduction of O_2 to O_2^{2-} are expected to be accompanied by a significant volume collapse, partly due to intrinsic and solvational volume changes. It was assumed that the rate determining step within a whole sequence of steps must be the attack of dioxygen on the first copper(I) ion, accompanied by an electron transfer step (leading formally to a copper(II) superoxo complex). This species then reacts very quickly to produce the peroxo complex and then again in a fast reaction sequence to give the product. The negative $\Delta V^{\#}$ value found for the oxidation of the dinuclear copper complex is close to the average value of -22 ± 2 cm^3 mol^{-1} reported for the oxidation of $Cu^{I}(phen)_2$ by dioxygen [58]. In the latter study it was concluded that the significantly negative volume of activation mainly arises from the large volume reduction associated with the formation of the intermediate $(phen)_2Cu^{I}$–O_2 species.

In other studies performed in our laboratories, it was found that the mononuclear copper(I) complex with the tripodal amine ligand Me_6tren (tris(2-dimethylaminoethyl)amine) reacts reversibly with oxygen at low temperatures to form superoxo and peroxo complexes [59]. The reaction could be followed by employing a low temperature stopped-flow instrument and the spectral changes that occurred during the formation of the superoxo complex ($\lambda_{max} = 412$ nm) at -90°C are shown in Fig. 8. The formation of the superoxo species was much faster at higher temperatures and so only its decomposition along with the formation of the peroxo complex could be observed.

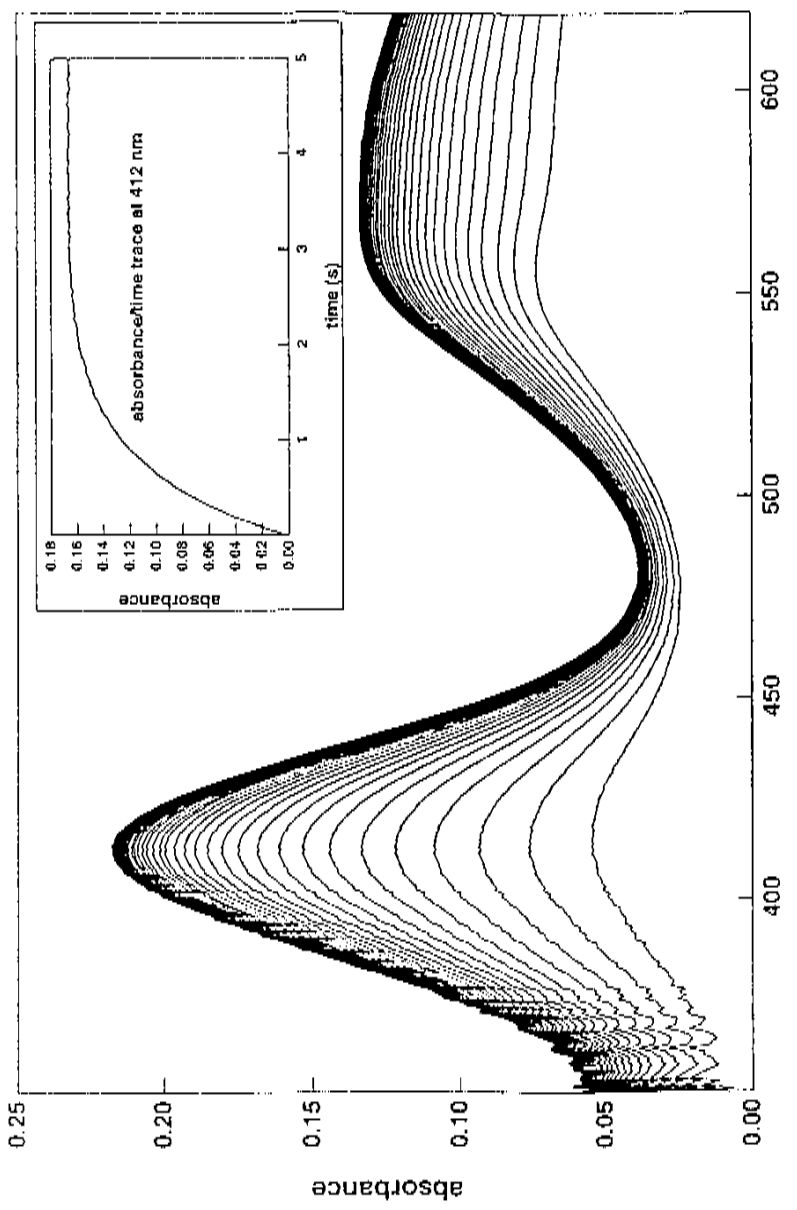

Fig. 8. Reaction of $[Cu(Me_6tren)(CH_3CN)]PF_6$ with dioxygen at −90°C in dry propionitrile. The insert shows the absorbance versus time trace at 412 nm [59].

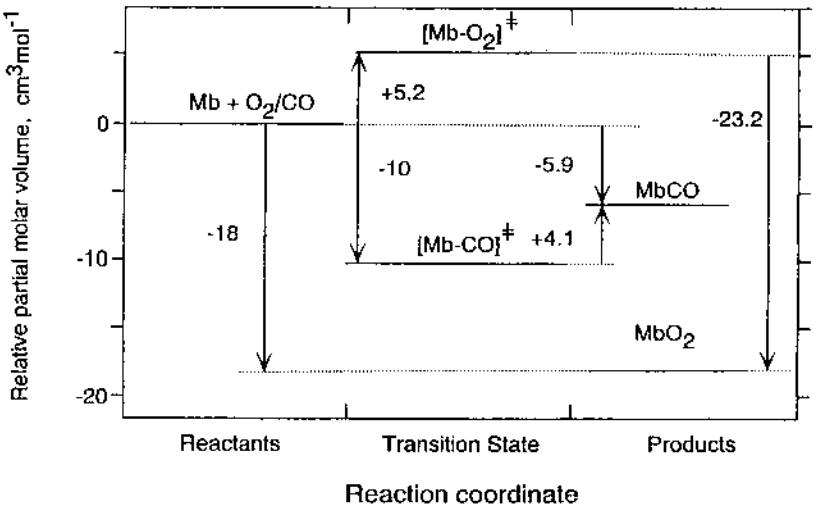

Fig. 9. Volume profiles for the reactions of O_2 and CO with myoglobin [60].

3.2. Activation of carbon monoxide

The binding of CO has been used in many studies as a model for the activation of dioxygen, since this molecule does not undergo any real activation in the systems studied, it merely binds to the metal center. The absence of subsequent electron transfer reactions simplifies the kinetic analysis and reveals more mechanistic insight on the actual binding process.

A typical example concerns the comparative binding of O_2 and CO to deoxymyoglobin [60]. The large difference in $\Delta V^{\#}$ observed for these reactions can clearly be seen from the comparative volume profiles shown in Fig. 9. The volume profile for the binding of O_2 is characterised by a substantial increase in volume in going from the reactant to the transition state, followed by a significant volume reduction on going to the product state. The observed volume increase was ascribed to the rate-determining movement of O_2 through the protein to the heme pocket, which may involve hydrogen bonding to the distal histidine as well as desolvation. This step is followed by rapid bond formation with the Fe(II) center, during which the change in spin state from high to low, the movement of the Fe(II) center into the porphyrin plane, and the associated conformational changes account for the drastic volume reduction. The overall reaction volume of -18 cm^3 mol^{-1} demonstrates the large volume reduction caused by the binding of O_2. The volume profile for the binding of CO shows a considerable volume decrease on going from the reactant to the transition state, which has been ascribed to rate-determining bond formation. The reverse bond cleavage reaction is accompanied by a volume decrease, which may be related to the different bonding mode of CO compared with O_2. This difference in bonding mode must also account for the much smaller absolute reaction volume observed in this case.

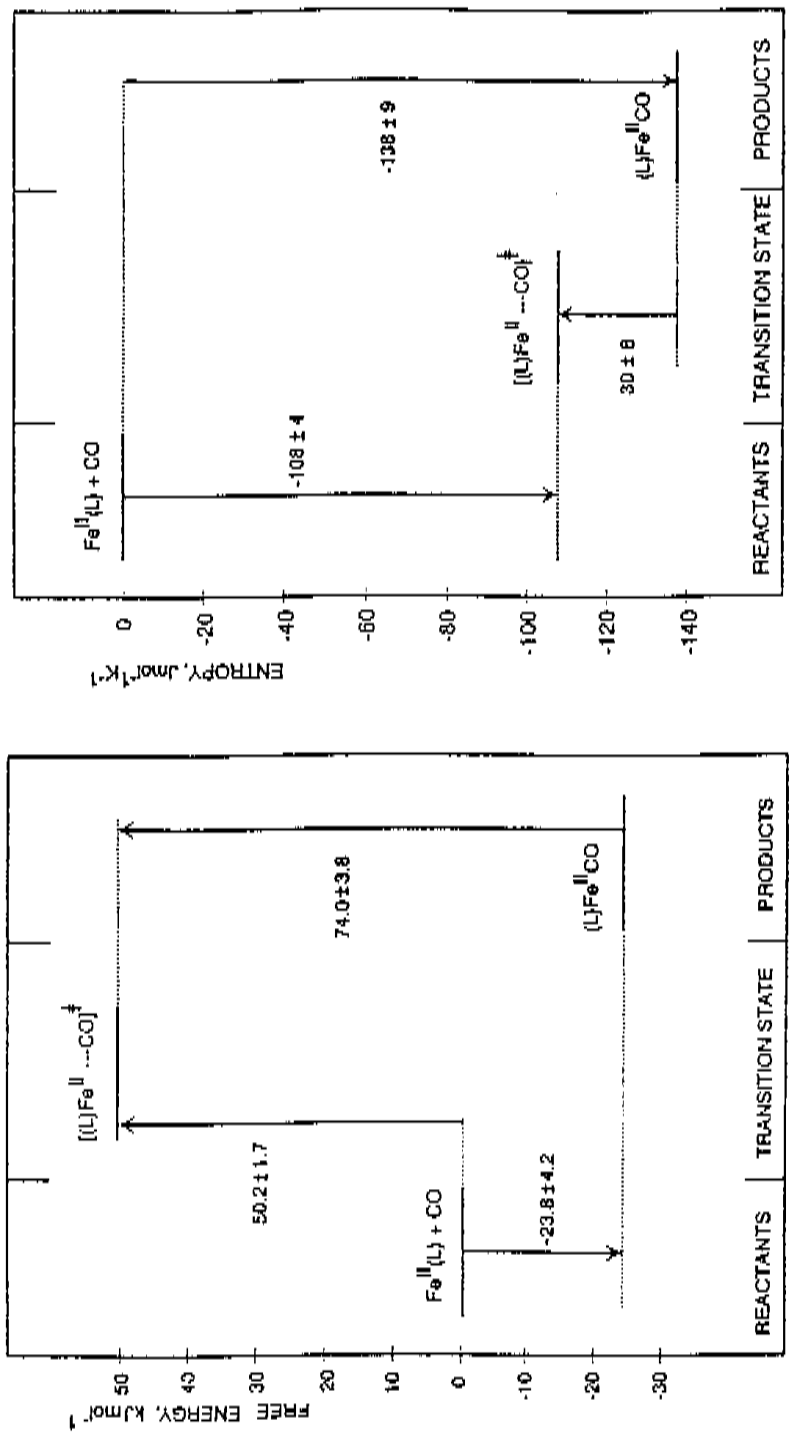

Fig. 10. Free energy and entropy diagrams for the reaction of $[Fe^{II}(PhBzXy)](PF_6)$ with CO in acetonitrile [62].

In another study the binding of CO to LACUNAR Fe(II) complexes was studied in detail as a function of temperature and pressure [61,62]. In these systems the high spin Fe(II) center is five-coordinate and has a vacant pocket available for the binding of CO. These systems can therefore be considered as ideal for the modelling of biological processes. A detailed kinetic analysis of the on and off reactions, as well as a thermodynamic analysis of the overall equilibrium, enabled the construction of the energy and volume profiles for the binding of CO to $[Fe^{II}(PhBzXy)](PF_6)_2$ shown in Figs. 10 and 11, respectively [62]. The free energy profile demonstrates the favourable thermodynamic driving force for the overall reaction, as well as the relatively low activation energy for the binding process. The entropy profile demonstrates the high degree of order in the transition state on the binding of CO. The large volume collapse associated with the forward reaction (Fig. 11) is very close to the partial molar volume of CO, which suggests that CO completely disappears within the ligand pocket cavity of the complex in the transition state during partial Fe–CO bond formation. It is known also [61] that Fe^{II}–CO bond formation is accompanied by a high-spin to low-spin conversion of

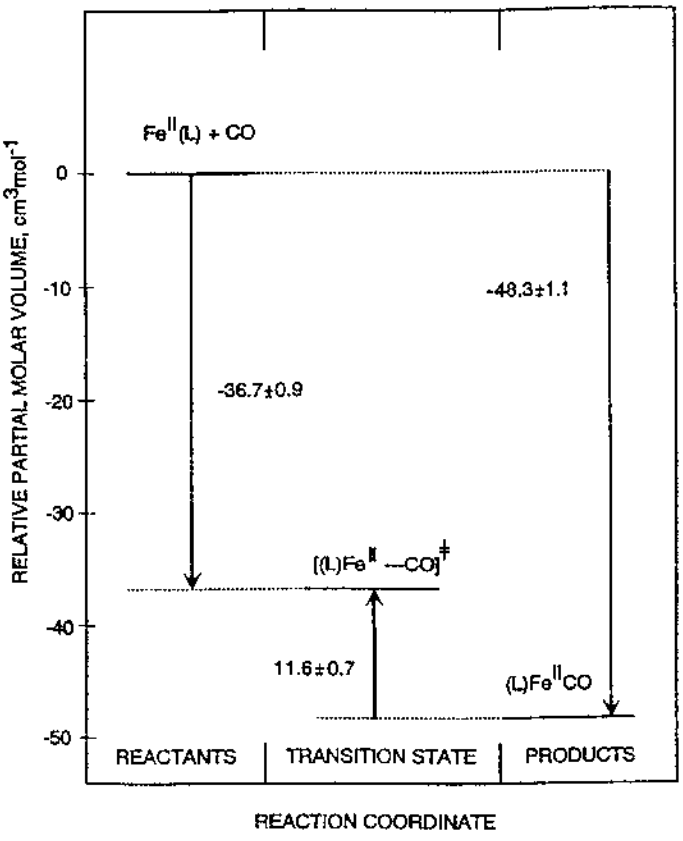

Fig. 11. Volume profile for the reaction of $[Fe^{II}(PhBzXy)](PF_6)$ with CO in acetonitrile [62]

.

the Fe(II) center. In forming the six-coordinate, low-spin Fe(II) complex, the metal moves toward the plane of the equatorial nitrogen donors. Thus following the transition state for the binding of CO, there is a high-spin to low-spin change during which bond formation is completed and the metal center moves into the ligand plane. These processes account for the subsequent volume decrease observed from the transition to the product state. The overall reaction volume of -47 cm^3 mol^{-1} therefore consists of a volume decrease of ca. -35 cm^3 mol^{-1} associated with the disappearance of CO into the ligand cavity, and ca. -12 cm^3 mol^{-1} for the high-spin to low-spin transition.

3.3. Activation of carbon dioxide

One of the most fundamental processes dealing with the activation of CO_2, involves the hydration of CO_2 to produce bicarbonate, as well as the reverse dehydration of bicarbonate to produce CO_2. These processes are of biological and environmental interest since they control the transport and equilibrium behaviour of CO_2. The spontaneous hydration of CO_2 and dehydration of HCO_3^- are processes that are too slow and must therefore be catalyzed by metal complexes in order to expedite the overall conversion rate. In biological systems, enzymes are the efficient catalysts, and we have undertaken some studies to clarify the catalytic mechanism of such systems.

The active centre of the zinc containing metalloenzyme carbonic anhydrase (CA) consists of three histidine residues and one water molecule coordinated to zinc in a slightly distorted tetrahedral geometry. Catalytic activity is integrally related to the ionisation (pK_a value ca. 7) of the coordinated water molecule, and for human CA II the mechanism is referred to as the zinc hydroxide mechanism, which has been described and modelled theoretically in considerable detail [63]. According to this mechanism it is the hydroxo form of the enzyme that can bind CO_2 to produce a bicarbonato complex, which subsequently undergoes a ligand exchange reaction with water to rapidly release HCO_3^-. During the reverse dehydration reaction, it is the aqua form of the enzyme that is the reactive species, rapidly binds HCO_3^- via a substitution of coordinated water, followed by decarboxylation to release CO_2. Thus the hydration and dehydration reactions exhibit very characteristic pH dependences. Model complexes must therefore on the one hand mimic the active site of the enzyme, and on the other hand exhibit the characteristic pH dependence observed in the catalytic activity of the enzyme.

The first model complex that could adhere to both these requirements was the triazacyclododecane complex of Zn(II), viz. Zn([12]aneN$_3$)H$_2$O^{2+}, which has a pK_a value of 7.3 [64]. The pH dependence of both the hydration and dehydration reactions is presented schematically in Fig. 12, from which it clearly follows that only the hydroxo complex catalysis the hydration of CO_2, and only the aqua complex catalysis the dehydration of HCO_3^-. A significantly higher catalytic activity was found for the five-coordinate tetraazacyclododecane complex, viz. Zn([12]aneN$_4$)H$_2$O^{2+}, which has a pK_a value of 8.0 [65]. Both the hydration and dehydration rate constants of this model catalyst were between five and six times

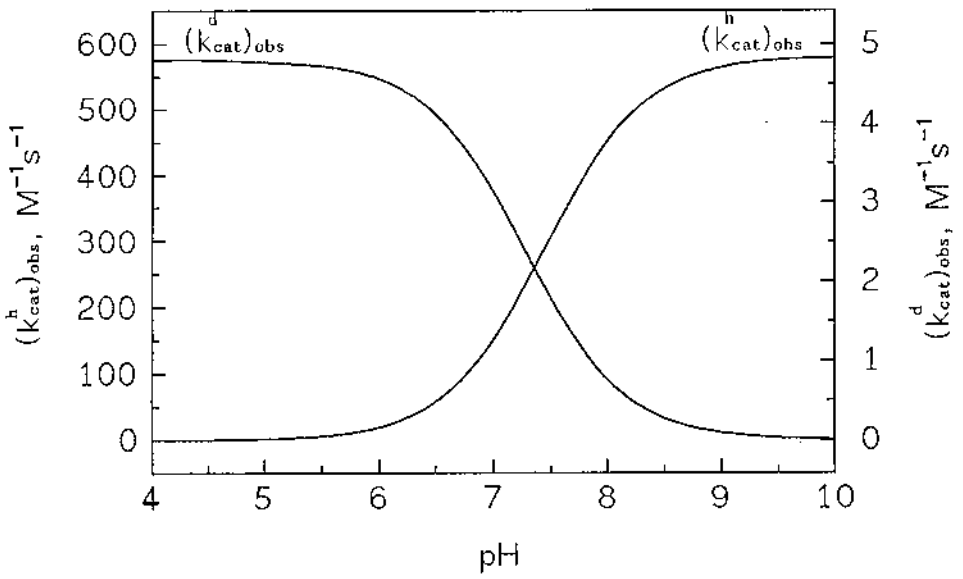

Fig. 12. pH profiles for the Zn([12]aneN$_3$)-catalyzed hydration (h) of CO_2 and dehydration (d) of HCO_3^- at 298 K [64].

higher than for the four-coordinate triazacyclododecane complex. This is associated with the possibility that the four coordinate complex can stabilize the bicarbonate intermediate through ring-closure, something that is not possible for the five-coodinate complex, and thus its higher catalytic activity [65]. The ability of these simple coordination compounds to mimic the catalytic activity of CA is impressive, but their actual reactivity is still orders of magnitude below that of CA.

The CA catalyzed reactions themselves have been studied in detail by many investigators using a wide variety of techniques, and have formed the subject of several theoretical calculations and computer simulations [63]. The application of high pressure kinetic measurements provided further mechanistic distinction than previously available [66]. A gratifyingly close agreement was obtained between the reaction volume for the uncatalyzed reaction obtained earlier [67] and that derived from kinetic measurements on the catalyzed reaction in both directions. The first complete, detailed volume profile (see Fig. 13) for an enzyme catalyzed reaction could be generated. The Zn(II) bound hydroxyl moiety subjects the carbon of CO_2 to nucleophilic attack resulting in the formation of an oxygen–carbon bond, and the results are consistent with a unidentate bonding of bicarbonate. For this process the transition state lies approximately halfway between the reactant and product states (see left part of volume profile). The substitution of coordinated bicarbonate by water tends more toward a limiting D mechanism (see right part of volume profile) than would be predicted on the basis of the coordination chemistry of aquated Zn(II), which may result from the influence of the environment of the active centre of the enzyme.

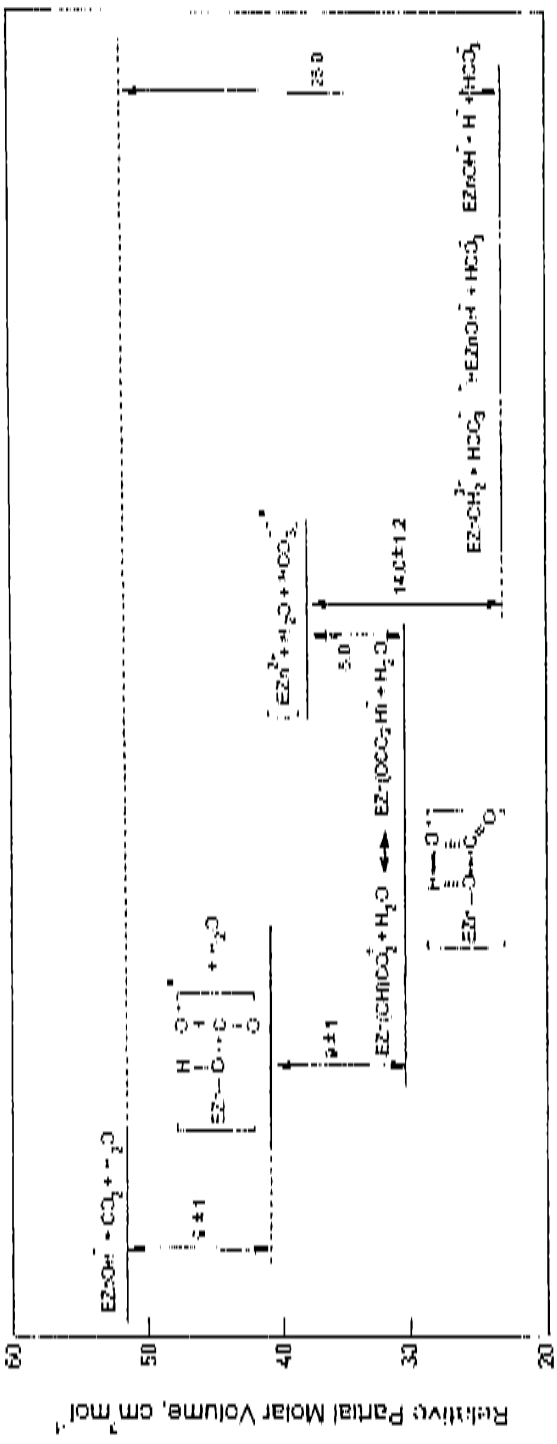

Fig. 13. Volume profile for the carbonic anhydrase catalyzed hydration of CO_2 and dehydration of HCO_3^- [66].

A logical challenge would be to use similar model catalysts for the reaction of CO_2 with alcohols instead of water in order to produce organic carbonates without the usage of phosgene. We performed detailed studies on the tetraazacyclododecane Zn(II) system discussed above in methanol and other alcohols as solvent in efforts to catalyse the formation of mono- and dialkylcarbonates. We found structural evidence for the coordination of ethanol to this Zn(II) complex, and isolated a trinuclear carbonato bridged complex, $\{[Zn([12]aneN_4)]_3(\mu_3\text{-}CO_3)\}(ClO_4)_4$ [68]. This complex seems to be a poorly soluble dead end species en route to the formation of dialkylcarbonates.

Fujita et al. [69] and others have used a wide range of methods to study cobalt(I) complexes with tetraazamacrocyclic ligands as potential catalysts for the reduction of CO_2. The interaction of the low spin $[Co^{I}HMD]^+$ species, HMD = 5,7,7,12,14,14-hexamethyl-1,4,8,11-tetraazacyclotetradecane-4,11-diene, with CO_2 in CH_3CN leads to a five-coordinate species, $[CoHMD(CO_2)]^+$, which is in equilibrium with a six-coordinate complex ion, $[CoHMD(CO_2)\text{-}(CH_3CN)]^+$, formed through addition of CH_3CN. Results from an XANES study together with other information provide a clear indication that in the six-coordinate complex cobalt is in the $+3$ oxidation state, meaning that the complex ion is Co(III)-CO_2^{2-} (i.e. CO_2 is coordinated as carboxylate). Hence the initial cobalt(I) complex has reduced the bound CO_2 to carboxylate. The change in coordination number equilibrium can be studied readily by UV–vis spectrophotometry; the thermodynamic parameters are $\Delta H° = -29$ kJ mol^{-1}, $\Delta S° = -113$ J mol^{-1} K^{-1} and $\Delta V° = -17.7$ cm^3 mol^{-1}. The latter two are mutually compatible and consistent with a highly ordered and compact six-coordinate complex ion. It has been proposed that a major part of the volume decrease arises from the intramolecular electron transfer process accompanied by a shortening of the Co–CO_2 bond (as supported by XANES and EXAFS studies) and an increase in electrostriction. Only a relatively minor contribution to the large negative reaction volume is suggested to result from the intrinsic effect of CH_3CN addition [69].

Other studies undertaken in our laboratories concerned the activation of CO_2 by complexes of Ni(0). Even though it is well known that Ni(0)-complexes can react with carbon dioxide (a structurally characterized carbon dioxide complex was synthesized from a Ni(0)-compound), our results showed that the complex [Ni(bpy)(COD)] is unreactive towards carbon dioxide. For the reaction of [Ni(bpy)(COD)] with propionaldehyde and carbon dioxide, a thorough kinetic study clearly demonstrated that carbon dioxide does not bind to the Ni(0) center but instead reacts with the activated propionaldehyde of the complex [Ni(bipy)(propionaldehyde)] to produce a cyclic organocarbonate [70].

3.4. Activation of sulfur dioxide

The coordination chemistry of sulfur dioxide exhibits a remarkable resemblence with that of carbon dioxide. A number of research groups have over the past years concentrated their studies on the possible role of transition metal ions and complexes in the aqueous phase chemistry of SO_2 in atmospheric waters, i.e. cloud

and rain water. The work has focused mainly on the catalytic role of metal ions and complexes in the autoxidation of sulfur(IV) oxides, during which sulfuric acid and sulfates are produced that lead to the formation of acid rain. In general it is accepted that such reactions contribute to the acidification of cloud and fog water in the atmosphere [71]. Although the overall chemical processes involved in such oxidation processes are quite complex, it is in principle possible to focus on some elementary reaction steps that assist the elucidation of the autoxidation mechanism and the catalytic role of the metal ions.

Numerous studies have dealt with transition metal catalyzed oxidation of sulfur(IV) oxides and recent reviews focus on atmospheric relevant processes and mechanisms, and the particular role of coordination chemistry in such processes [72,73]. Other metals that are considered as potential catalysts are manganese, cobalt and copper [71,72]. Of all these systems, the catalytic role of iron and manganese has been studied in much detail and a more complete treatment of the available data will be given. Our own work has focused on the catalytic role of iron ions and complexes in the autoxidation reactions of sulfur(IV) oxides.

Kinetic investigations were first performed at a pH of 2.5. Under these conditions the main reactive species in solution were found to be $Fe(H_2O)_6^{3+}$, $Fe(H_2O)_5OH^{2+}$, SO_2 and HSO_3^-. A detailed study of the complex-formation reactions using conventional and rapid-scan UV–vis techniques [74], demonstrated that 1:1, 1:2 and 1:3 Fe(III)–S(IV) complexes are formed rapidly in three subsequent steps in solution, prior to the subsequent redox processes. The kinetics of the complex-formation reactions clarified that the main reactive species are $Fe(H_2O)_5OH^{2+}$ and HSO_3^-, which produce the mentioned complexes. In later work [75] it was claimed that only an 1:1 complex is formed in solution. However, a detailed reinvestigation using more sophisticated rapid-scan equipment [76] showed clearly that our original claim [74] was perfectly correct.

Subsequently, the redox reactions of the various Fe(III)–S(IV) complexes were investigated in detail. The kinetic traces indicated the occurrence of at least two subsequent reaction steps in argon saturated solutions, with an even more complex behavior in the case of air or oxygen saturated solutions [74]. In the absence of oxygen, the oxidation of sulfite to sulfate is induced by the reduction of Fe(III) to Fe(II), where polymeric Fe(III) hydroxo species were suggested to account for the subsequent slow decomposition reactions.

In the presence of oxygen and sulfite, direct evidence for the redox cycling of Fe(II/III) was found [77]. Typical kinetic traces recorded in the presence of oxygen exhibited in addition to the complex-formation and subsequent redox reactions mentioned above, direct evidence for the redox cycling of Fe(II/III) under such conditions. The traces (Fig. 14) exhibited a clear break point which could be correlated with the rapid reoxidation of Fe(II) in the presence of oxygen and sulfite, up to the point that all dissolved oxygen in solution had been used. The observed kinetic traces could be fitted to a reaction mechanism that consists of the reactions (1–11) [78].

$$FeOH^{2+} + HSO_3^- \rightleftarrows [Fe(OH)HSO_3]^+ \quad (1)$$

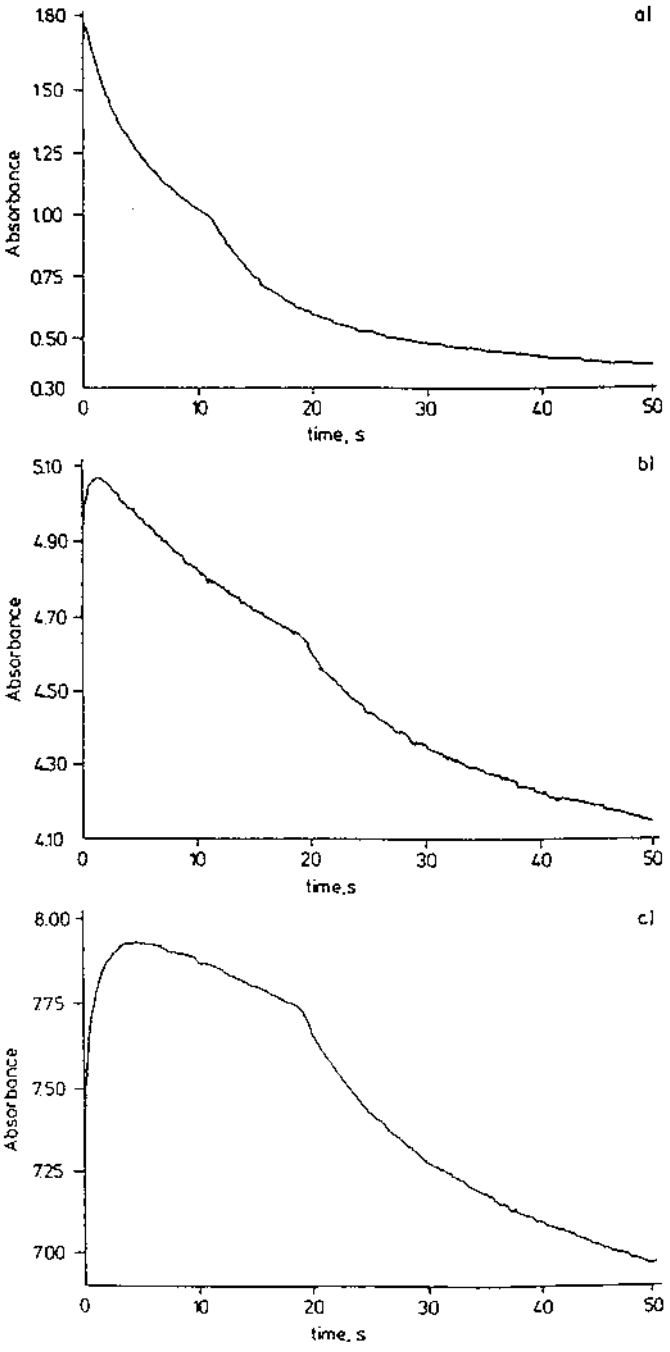

Fig. 14. Typical kinetic traces recorded at 390 nm for the Fe(III) catalyzed autoxidation of S(IV) oxides. (a) [Fe(II)] = 0 M; (b) [Fe(II)] = 1×10^{-4} M; (c) [Fe(II)] = 5×10^{-4} M. Further experimental details are given in Ref. [78].

$$[Fe(OH)HSO_3]^+ \rightarrow Fe^{2+} + SO_3^- + H_2O \quad (2)$$

$$SO_3^- + O_2 \rightarrow SO_5^- \quad (3)$$

$$Fe^{2+} + SO_5^- + H_2O \rightarrow FeOH^{2+} + HSO_5^- \quad (4)$$

$$Fe^{2+} + HSO_5^- \rightarrow FeOH^{2+} + SO_4^- \quad (5)$$

$$Fe^{2+} + SO_4^- \rightarrow Fe^{3+} + SO_4^{2-} \quad (6)$$

$$SO_5^- + HSO_3^- \rightarrow HSO_5^- + SO_3^- \quad (7)$$

$$SO_5^- + HSO_3^- \rightarrow SO_4^{2-} + SO_4^- + H^+ \quad (8)$$

$$SO_4^- + HSO_3^- \rightarrow SO_4^{2-} + SO_3^- + H^+ \quad (9)$$

$$SO_5^- + SO_5^- \rightarrow S_2O_8^{2-} + O_2 \quad (10)$$

$$HSO_5^- + HSO_3^- + H^+ \rightarrow 2SO_4^{2-} + 3H^+ \quad (11)$$

The initiation reactions (1) and (2) are suggested to involve different iron–sulfito complexes as mentioned above. Reaction (4) is a crucial step since it accounts for the reoxidation of the reduced Fe(II) species with SO_5^- being a strong oxidant. Warneck and co-workers [79,80] provided evidence for the participation of SO_4^- radicals during the Fe(III) catalyzed autoxidation of S(IV) oxides. No evidence for the participation of·OH radicals could be found. Simulations of this mechanism based on available rate constants, indicated that the reoxidation routes via SO_4^- and HSO_5^- are too slow to contribute meaningfully, such that SO_5^- must be mainly responsible for the reoxidation of Fe(II). The available experimental results largely support the proposed mechanism.

The catalytic effect displayed by manganese(II/III) was studied in considerable detail by Elding and co-workers [81]. The reaction was shown to be autocatalytic with an induction period. The latter could be shown to be due to the formation of manganese(III), which is the actual catalyst similar to the case of iron(III). In the absence of initially added Mn(III) it was proposed that low concentrations of iron(III), present as unavoidable impurities at levels of 10^{-8} mol dm^{-3}, are responsible for the initiation of the reaction. A simplified reaction mechanism, rather similar to the one given above for the iron-catalyzed reaction, can be written as follows [81]:

$$Mn^{2+} + HSO_3^- \rightleftarrows MnHSO_3^+ \quad (12)$$

$$Mn(III) + MnHSO_3^+ \rightarrow 2Mn(II) + SO_3^- + H^+ \quad (13)$$

$$SO_3^- + O_2 \rightarrow SO_5^- \quad (14)$$

$$Mn(II) + SO_5^- + H^+ \rightarrow Mn(III) + HSO_5^- \quad (15)$$

$$Mn(II) + HSO_5^- \rightarrow Mn(III) + SO_4^{2-} + OH \quad (16)$$

$$MnHSO_3^+ + HSO_5^- \rightarrow Mn(II) + 2HSO_4^- \quad (17)$$

$$MnHSO_3^+ + OH \rightarrow Mn(II) + SO_3^- + H_2O \quad (18)$$

These steps are followed by reactions (7–11) as given above. The redox cycling of manganese is an essential component of the catalytic process. The $MnHSO_3^+$ species was suggested to be the reactive complex in the above outlined mechanism.

A laboratory demonstration experiment was developed on the basis of the general observations for one-electron metal oxidants [82]. A general mechanism based on the detailed kinetic studies referred to above is presented in Fig. 15 and illustrates the important role of redox cycling of the metal ion in such catalytic processes.

3.5. Activation of nitrogen oxides

Nitrogen oxides, as well as mixed sulfur–nitrogen oxides, produced during the spontaneous or metal catalyzed interaction of $NO/HONO/NO_2^-$ with $SO_2/HSO_3^-/SO_3^{2-}$, can interact with metal ions and complexes and affect their oxidation state. Such reactions can play an important role in the treatment of gaseous effluents from coal-fired power plants, as well as in atmospheric oxidation processes. In general, iron(II) complexes can rapidly bind NO to produce species of the type $Fe(III)–NO^-$, which decompose to iron(III) and NO^-, i.e. N_2O. Coordinated NO can interact with bisulfite to produce hydroxylamine-disulfonate(HADS), N_2O and iron(III) [83,84]. It has also been reported that the reaction between nitrous acid and bisulfite is a potential source of free radicals in natural environments [85]. Manganese(III) and iron(III) ions and complexes can affect the hydrolysis reactions of such mixed sulfur–nitrogen oxides [86]. For instance, HADS hydrolyzes rapidly under such conditions to hydroxylaminemonosulfonate, during which the metal ions are reduced to the $+2$ oxidation state. In one case evidence for the redox cycling of manganese(II/III) in the presence of a sulfur–nitrogen oxide was observed [87]. The role of these reactions in atmospheric oxidation processes is presently unknown despite their potential importance, especially in terms of controlling the oxidation state of the catalytic metal ions [88–91].

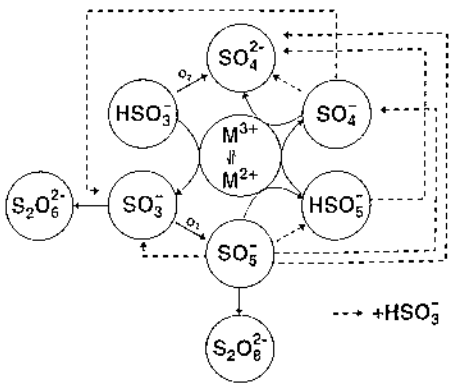

Fig. 15. Generalized reaction scheme, showing the role of one electron metal oxidants in the oxidation of sulfur(IV) in aqueous solution.

4. Electron transfer reactions

Some of the systems described in Section 3 demonstrated already the important role played by electron transfer reactions in the activation of small molecules. Such activation processes include in many cases a combination of substitution and electron transfer reactions as essential steps. In this section we want to focus on the electron transfer reactions themselves and some of the mechanistic studies we have performed in recent years. Some of our work in this area involving the application of high pressure kinetic and thermodynamic techniques was reviewed as part of a special symposium devoted to the complementarity of various experimental techniques in the study of electron transfer reactions [92]. One of the most exciting areas that we have been involved in through collaborations with J.F. Wishart (Brookhaven National Laboratory) and H.B. Gray (California Institute of Technology) has dealt with the effect of pressure on long distance electron transfer reactions, and an account of this work will be included here.

It has in general been the objective of many mechanistic studies dealing with inorganic electron transfer reactions to distinguish between outer-sphere and inner-sphere mechanisms. Along these lines high pressure kinetic methods and the construction of reaction volume profiles have also been employed to contribute towards a better understanding of the intimate mechanisms involved in such processes. The differentiation between outer-sphere and inner-sphere mechanisms depends on the nature of the precursor species, Ox//Red in the following scheme, which can either be an ion pair or encounter complex, or a bridged intermediate, respectively.

$$\mathrm{Ox} + \mathrm{Red} \leftrightarrows \mathrm{Ox//Red}, \quad K$$

$$\mathrm{Ox//Red} \rightarrow \mathrm{Ox}^- // \mathrm{Red}^+, \quad k_{\mathrm{ET}}$$

$$\mathrm{Ox}^- // \mathrm{Red}^+ \rightleftarrows \mathrm{Ox}^- + \mathrm{Red}^+$$

This means that the coordination sphere of the reactants remains intact in the former case and is modified by ligand substitution in the latter, which will naturally affect the associated volume changes.

We have in our earlier work concentrated mainly on the analysis of non-symmetrical electron transfer reactions [93], i.e. reactions in which redox products are formed and for which the overall driving force and reaction volume will not be zero. Some typical examples of such studies will be discussed in more detail to form a basis for the subsequent section dealing with long distance electron transfer processes.

A general difficulty encountered in kinetic studies of outer-sphere electron transfer processes concerns the separation of the precursor formation constant (K) and the electron transfer rate constant (k_{ET}) in the scheme outlined above. In the majority of cases, precursor formation is a diffusion controlled step, followed by rate-determining electron transfer. In the presence of an excess of Red, the rate expression is given by

$$k_{obs} = k_{ET}K[\text{Red}]/(1 + K[\text{Red}])$$

In many cases K is small, such that this equation simplifies to $k_{obs} = k_{ET}K[\text{Red}]$, which means that the observed second-order rate constant and the associated activation parameters are composite quantities, viz. $\Delta V^{\#} = \Delta V^{\#}(k_{ET}) + \Delta V(K)$. When K is large enough such that $1 + K[\text{Red}] > 1$, it is possible to separate k_{ET} and K kinetically and also the associated activation parameters, viz. $\Delta V^{\#}(k_{ET})$ and $\Delta V(K)$ [93].

One of the first systems investigated concerned the redox reaction between $Co(terpy)_2^{2+}$ and $Co(bipy)_3^{3+}$ in different solvents [94]. Due to the similar charge on these species, K for ion-pair formation in terms of an outer-sphere mechanism is very small and the observed $\Delta V^{\#}$ is a composite quantity. The reported activation volumes for the investigated solvents are -9.4 (H_2O), -13.8 ($HCONH_2$) and -5.1 (CH_3CN) cm^3 mol^{-1}. Theoretical calculations based on the Marcus–Hush relationships resulted in a $\Delta V^{\#}$ value of -7.3 cm^3 mol^{-1} for the reaction in water, which is indeed close to the experimental value.

A series of reactions were studied where it was possible to resolve K and k_{ET}, i.e. $\Delta V(K)$ and $\Delta V^{\#}(k_{ET})$. In this case oppositely charged reaction partners were selected as indicated in the following scheme [95–97]:

$$Co(NH_3)_5X^{(3-n)+} + Fe(CN)_6^{4-} \rightleftarrows [Co(NH_3)_5X^{(3-n)+}\cdot Fe(CN)_6^{4-}], \quad K$$

$$[Co(NH_3)_5X^{(3-n)+}\cdot Fe(CN)_6^{4-}] \rightarrow [Co(NH_3)_5X^{(2-n)+}\cdot Fe(CN)_6^{3-}], \quad k_{ET}$$

$$[Co(NH_3)_5X^{(2-n)+}\cdot Fe(CN)_6^{3-}] \rightarrow Co^{2+} + 5NH_3 + X^{n-} + Fe(CN)_6^{3-}, \quad \text{fast}$$

where $X^{n-} = H_2O$, Me_2SO, py, Cl^-, N_3^-.

The thermodynamic parameters for ion-pair formation indicated that ion-pair formation did not only depend on the charge of the participating species, but that other types of interactions must be considered to account for the trend in the values of K. Throughout the series, ion-pair formation is accompanied by significantly negative $\Delta S°$ values and close to zero ΔV values. The latter is rather surprising, since it is generally accepted that ion-pair formation should involve considerable charge neutralization accompanied by strong desolvation due to a decrease in electrostriction. The values of ΔV therefore indicate that the reaction partners most probably exist as solvent-separated ion-pairs, i.e. with no significant charge neutralization accompanied by desolvation.

The electron transfer step exhibited a strong pressure deceleration, most systems had a $\Delta V^{\#}$ value of between $+25$ and $+34$ cm^3 mol^{-1}. These values indicate that electron transfer is accompanied by extensive desolvation, most probably related to charge neutralization associated with the electron transfer process [97]. A simplified model based on partial molar volume data, in which electron transfer occurs from the precursor ion pair $[Co(NH_3)_5X^{(3-n)+}\cdot Fe(CN)_6^{4-}]$ to the successor ion pair $[Co(NH_3)_5X^{(2-n)+}\cdot Fe(CN)_6^{3-}]$, predicted an overall volume increase of ca. 65 cm^3 mol^{-1}. This means that according to the reported $\Delta V^{\#}$ values the transition state for the electron transfer process lies approximately halfway between the reactant and product states on a volume basis for the precursor and successor ion pairs. The

largest volume contribution arose from the oxidation of $Fe(CN)_6^{4-}$ to $Fe(CN)_6^{3-}$, which is accompanied by a large decrease in electrostriction and an increase in partial molar volume. Similar data were also reported for a series of related complexes containing phosphor-oxo ligands [98,99]. The results could be interpreted in terms of major solvational changes associated with the oxidation of $Fe(CN)_6^{4-}$.

This first information on the nature of the volume profile for an outer-sphere electron-transfer reaction proved to be in good agreement with subsequently reported results for systems with low driving forces, in which it was possible to construct a complete volume profile by studying the effect of pressure on both the forward and reverse reactions, as well as on the overall equilibrium constant (see further discussion on redox reactions involving cytochrome *c*).

A challenging question concerns the feasibility of the application of high pressure kinetic and thermodynamic techniques in the study of long distance electron transfer reactions. Do such processes exhibit a characteristic pressure dependence, and to what extent can a volume profile analysis reveal information on the intimate mechanism of the electron transfer process?

The systems that we investigated in collaboration with others involved intermolecular and intramolecular electron transfer reactions between ruthenium complexes and cytochrome *c*. We also studied a series of intermolecular reactions between chelated cobalt complexes and cytochrome *c*. A variety of high pressure experimental techniques, including stopped-flow, flash-photolysis, pulse-radiolysis and voltammetry, were employed in these investigations. As the following presentation will show, a remarkably good agreement was found between the volume data obtained with the aid of these different techniques, which clearly demonstrates the complementarity of these methods for the study of electron transfer processes.

Application of pulse-radiolysis techniques revealed that the following intramolecular and intermolecular electron transfer reactions all exhibit a significant acceleration with increasing pressure.

$$(NH_3)_5Ru^{II}\text{–(His33)cyt } c^{III} \rightarrow (NH_3)_5Ru^{III}\text{–(His33)cyt } c^{II}$$

$$(NH_3)_5Ru^{II}\text{–(His39)cyt } c^{III} \rightarrow (NH_3)_5Ru^{III}\text{–(His39)cyt } c^{II}$$

$$Ru^{II}(NH_3)_6^{2+} + \text{cyt } c^{III} \rightarrow Ru^{III}(NH_3)_6^{3+} + \text{cyt } c^{II}$$

The reported volumes of activation are -17.7 ± 0.9, -18.3 ± 0.7 and -15.6 ± 0.6 $cm^3\ mol^{-1}$, respectively, and demonstrate clearly a significant volume collapse on going from the reactant to the transition state [100].

At this stage it was uncertain what the negative volumes of activation really meant since overall reaction volumes were not available. There was however data, now in the literature [101], that suggested that the oxidation of $Ru(NH_3)_6^{2+}$ to $Ru(NH_3)_6^{3+}$ is accompanied by a volume decrease of ca. 30 $cm^3\ mol^{-1}$, which would mean that the activation volumes quoted above could mainly arise from volume changes associated with the oxidation of the ruthenium redox partner.

In order to obtain further information on the magnitude of the overall reaction volume and the location of the transition state along the reaction coordinate, a

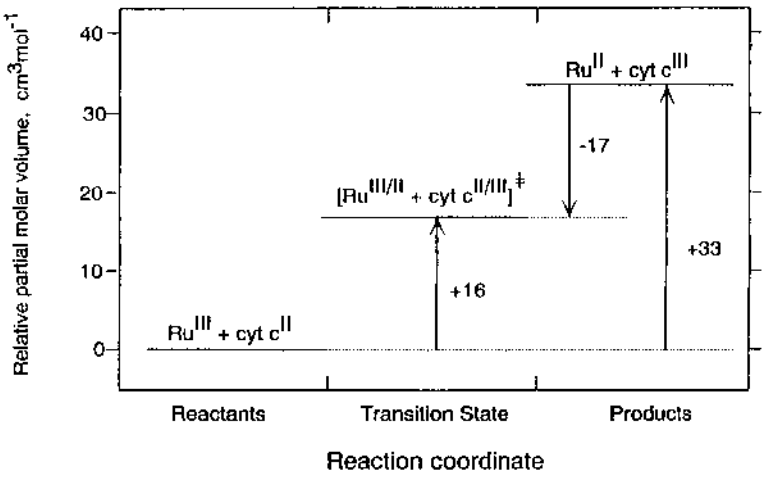

Fig. 16. Volume profile for the reaction [103]

$$Ru(NH_3)_5isn^{3+} + \text{cyt } c^{II} \leftrightarrows Ru(NH_3)_5isn^{2+} + \text{cyt } c^{III}.$$

series of intermolecular electron transfer reactions of cyt *c* with pentaammineruthenium complexes were studied, where the sixth ligand on the ruthenium complex was selected in such a way that the overall driving force was low enough so that the reaction kinetics could be studied in both directions [102,103]. The selected substituents were isonicotinamide (isn), 4-ethylpyridine (etpy), pyridine (py), and 3,5-lutidine (lut). The overall reaction can be formulated as

$$Ru^{III}(NH_3)_5L^{3+} + \text{cyt } c^{II} \leftrightarrows Ru^{II}(NH_3)_5L^{2+} + \text{cyt } c^{III}$$

For all the investigated systems, the forward reaction was decelerated significantly by pressure, whereas the reverse reaction was accelerated significantly by presssure. The absolute values of the volumes of activation for the forward and reverse processes were indeed very similar, demonstrating that a similar rearrangement occurs in order to reach the transition state. In addition, the overall reaction volume for these systems could be determined spectrophotometrically by recording the spectrum of an equilibrium mixture as a function of pressure, and electrochemically by recording cyclic and differential pulse voltammograms as a function of pressure [104]. These results are summarized along with the kinetic data and activation parameters in Table 1. A comparison of the ΔV data demonstrates the generally good agreement between the values obtained from the difference in the volumes of activation for the forward and reverse reactions, and those obtained thermodynamically. Furthermore, the values also demonstrate clearly that $|\Delta V^{\#}| \approx 0.5|\Delta V|$, i.e. the transition state lies approximately halfway between the reactant and product states on a volume basis independent of the direction of electron transfer. The typical volume profile in Fig. 16 presents the overall picture, from which the location of the transition state can clearly be seen.

Table 1
Summary of rate and activation parameters for the electron transfer reaction between cytochrome *c* and several pentaammineruthenium complexes [103]
$Ru^{III}(NH_3)_5L^{3+}$ + cyt c^{II} ⇆ $Ru^{II}(NH_3)_5L^{2+}$ + cyt c^{III}

Reaction	k (M^{-1} s^{-1})[a]	$\Delta H^{\neq}$ (kJ mol^{-1})	$\Delta S^{\neq}$ (JK^{-1} mol^{-1})	$\Delta V^{\neq}$ (cm^3 mol^{-1})	ΔV (cm^3 mol^{-1})	$-\Delta G$ (eV)	K_E [b]	K_{TD} [b]	K_{KIN} [b]
$Ru^{III}a_5$lutidine + cyt c^{II}	27144 ± 1271	35.4 ± 0.3	−41 ± 1	+16.9 ± 1.4	33.6 ± 1.7[c]	0.012	1.6	2.6 ± 0.1	2.9 ± 0.4
$R^{II}a_5$lutidine + cyt c^{III}	9448 ± 516	21 ± 1	−99 ± 5	−17.8 ± 1.6	34.7 ± 1.6[d]				
$Ru^{III}a_5$etpy + cyt c^{II}	26823 ± 477	29 ± 2	−61 ± 7	+14.7 ± 0.9	26.9 ± 1.8[c]	0.011	1.5	2.2 ± 0.4	2.9 ± 0.1
$Ru^{II}a_5$etpy + cyt c^{III}	9182 ± 124	25 ± 2	−86 ± 6	−14.9 ± 1.1	29.6 ± 1.0[d]				
$Ru^{III}a_5$py + cyt c^{II}	48620 ± 1161	28 ± 1	−64 ± 5	+17.4 ± 1.5	33.4 ± 1.9[c]	0.045	5.8	6.4 ± 2.1	4.6 ± 0.4
$Ru^{II}a_5$py + cyt c^{III}	10517 ± 494	33 ± 4	−59 ± 13	−17.7 ± 0.8	35.1 ± 1.0[d]				
$Ru^{III}a_5$isn + cyt c^{II}	1.15×10^5	22 ± 1	−75 ± 3	+16.0 ± 0.9	31 ± 1[c], 26.4 ± 0.9[e]	0.112	78	71 ± 7	75.7
$Ru^{II}a_5$isn + cyt c^{III}	1520 ± 130	28 ± 4	−87 ± 12	−17.2 ± 1.5	33.2 ± 1.3[d]				

[a] Reaction conditions: $T = 25°C$, $\mu = 0.1$ M, [cyt *c*] = 1×10^{-5} M, [Tris] = 0.05 M, [$LiClO_4$] = 0.05 M, pH 7.1, $\lambda = 550$ nm.
[b] Equilibrium constant for the oxidation of cytochrome *c*.
[c] Reaction volume determined spectrophotometrically for the oxidation of cytochrome *c*.
[d] Reaction volume determined kinetically for the oxidation of cytochrome *c*.
[e] Ref. [104].

Similar results were recently obtained for the redox reactions of a series of cobalt amine complexes with cytochrome *c*, for which the kinetic and thermodynamic parameters are summarized in Table 2 [105,106]. In general a good agreement exists between the parameters determined kinetically and thermodynamically, and the typical volume profile in Fig. 17 once again demonstrates the symmetrical location of the transition state with respect to the reactant and product states.

At this point it is important to ask the question where these volume changes really come from? We have always argued that the major volume change arises from changes on the redox partner and not on cytochrome *c* itself. This was suggested by the fact that the change in partial molar volume associated with the oxidation of the investigated Ru(II) and Co(II) complexes as obtained from electrochemical and density measurements, almost fully accounted for the observed overall reaction volume. Thus the reduction of cytochrome *c* can only make a minor contribution towards the overall volume change.

These arguments were apparently in contradiction with electrochemical results reported by Cruanes et al. [107], according to which the reduction of cytochrome *c* is accompanied by a volume collapse of 24 $cm^3\ mol^{-1}$. This value is so large that it almost represents all of the reaction volume found for the investigated reactions discussed above. A reinvestigation of the electrochemistry of cytochrome *c* as a function of pressure, using cyclic and differential pulse voltammetric techniques [104], revealed a reaction volume of $-14.0 \pm 0.5\ cm^3\ mol^{-1}$ for the reaction

$$\text{Cyt } c^{III} + Ag(s) + Cl^- \rightarrow \text{Cyt } c^{II} + AgCl(s)$$

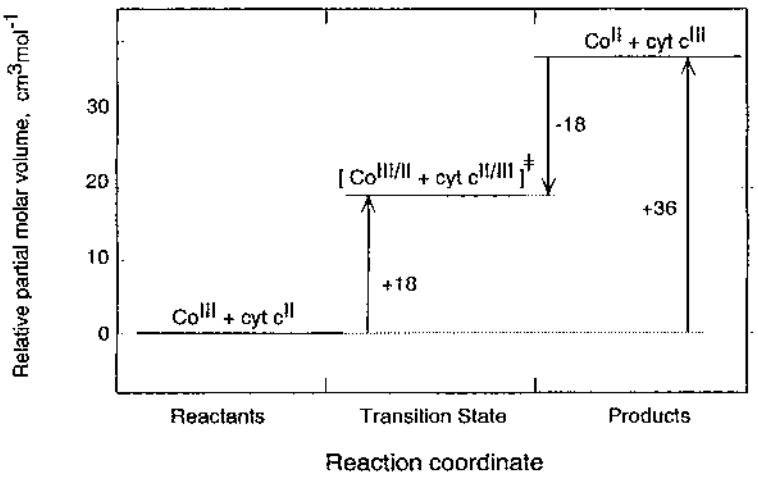

Fig. 17. Volume profile for the reaction [105]

$$Co(terpy)_2^{3+} + \text{cyt } c^{II} \leftrightarrows Co(terpy)_2^{2+} + \text{cyt } c^{III}.$$

Table 2
Summary of the rate and activation parameters for the electron transfer reaction between cytochrome *c* and several cobalt complexes [106]
$Co(L)^{3+} + cyt\ c^{II} \leftrightarrows Co(L)^{2+} + Cyt\ c^{III}$

Reaction	k ($M^{-1}\ s^{-1}$)[a]	$\Delta H^{\neq}$ (kJ mol^{-1})	$\Delta S^{\neq}$ ($JK^{-1}\ mol^{-1}$)	$\Delta V^{\neq}$ ($cm^3\ mol^{-1}$)	ΔV ($cm^3\ mol^{-1}$)	$-\Delta G$ (eV)	K_E [b]	K_{TD} [b]	K_{KIN} [b]
$Co(bpy)_3^{3+} + cyt\ c^{III}$	582 ± 13	49.9 ± 0.7	-28 ± 2	$+12.5 \pm 0.9$	21.8 ± 0.7[c]	0.028	3.0	3.3 ± 0.4	3.4 ± 0.3
$Co(bpy)_3^{2+} + cyt\ c^{III}$	169 ± 5	28 ± 1	-107 ± 5	-12.6 ± 1.5	25.1 ± 1.7[d]				
					27.5 ± 1.4[e]				
$Co(phen)_3^{3+} + cyt\ c^{II}$	3753 ± 39	44 ± 13	-28 ± 9	$+17.0 \pm 0.9$	37.9 ± 2.0[c]	0.085	32	20 ± 3	17.3 ± 0.6
$Co(phen)_3^{2+} + cyt\ c^{III}$	217 ± 5	14 ± 1	-136 ± 4	-16.2 ± 1.0	34.2 ± 1.7[d]				
					35.4 ± 2.0[e]				
$Co(terpy)_2^{3+} + cyt\ c^{II}$	1427 ± 36	40 ± 1	-47 ± 4	$+18.4 \pm 1.2$	33 ± 3[c]	−0.003	0.9	0.7 ± 0.2	0.9 ± 0.1
$Co(terpy)_2^{2+} + cyt\ c^{III}$	1704 ± 46	14 ± 1	-136 ± 4	-18.0 ± 1.4	36 ± 2[d]				
					36.3 ± 2.0[e]				

[a] Reaction conditions: $T = 25°C$, $\mu = 0.1$ M, [cyt *c*] $= 1 \times 10^{-5}$ M, [Tris] $= 0.05$ M, $[LiClO_4]/[LiNO_3] = 0.05$ M, pH 7.1, $\lambda = 550$ nm, $A = NH_3$.

[b] Equilibrium constant for the oxidation of cylochrome (K_E calculated from the redoxpotential, K_{TD} from spectroscopic measurements, K_{KIN} from kinetic measurements).

[c] Reaction volume determined spectrophotometrically for the oxidation of cytochrome *c*.

[d] Reaction volume determined kinetically for the oxidation of cytochrome *c*.

[e] Reaction volume determined electrochemically for the oxidation of cytochrome *c*.

A correction for the contribution from the reference electrode can be made on the basis of the data published by Tregloan et al. [108], and a series of measurements of the potential of the Ag | AgCl(KCl sat.) electrode relative to the Ag | Ag^+ electrode as a function of pressure. The contribution of the reference electrode turned out to be -9.0 ± 0.6 cm^3 mol^{-1}, from which it then followed that the reduction of cytochrome c^{III} is accompanied by a volume decrease of 5.0 ± 0.8 cm^3 mol^{-1}. This contribution is significantly smaller than concluded by Cruanes et al. [107] and is also in line with the other arguments referred to above. Thus we conclude that the observed activation and reaction volumes mainly arise from volume changes on the Ru and Co complexes, which in turn will largely be associated with changes in electrostriction in the case of the ammine complexes. The oxidation of the Ru(II) ammine complexes will be accompanied by a large increase in electrostriction and almost no change in the metal-ligand bond length, whereas in the case of the Co complexes a significant contribution from intrinsic volume changes associated with the oxidation of Co(II) will partially account for the observed effects [101].

The results in Tables 1 and 2 demonstrate nicely the complementarity of the kinetic and thermodynamic data obtained from stopped-flow, UV–vis, electrochemical and density measurements. The resulting picture is very consistent and allows a further detailed analysis of the data. The overall reaction volumes determined in four different ways are surprisingly similar and underline the validity of the different methods employed. The volume profiles in Figs. 16 and 17 demonstrate the symmetric nature of the intrinsic and solvational reorganization in order to reach the transition state of the electron transfer process. In these systems the volume profile is controlled by effects on the redox partner of cytochrome *c*, but this does not necessarily always have to be the case. The location of the transition state on a volume basis will reveal information concerning the early or late nature of the transition state and reveal details of the actual electron transfer route followed.

Recent investigations on a series of intramolecular electron transfer reactions, closely related to the series of intermolecular reactions described above, revealed non-symmetrical volume profiles [109]. Reactions of the type

$$(NH_3)_4(L)Ru^{III}\text{–(His33)–cyt } c^{II} \leftrightarrows (NH_3)_4(L)Ru^{II}\text{–(His33)–cyt } c^{III}$$

where L = isonicotinamide, 4-ethylpyridine, 3,5-lutidine, and pyridine, all exhibited volumes of activation for the forward reaction of between $+3$ and $+7$ cm^3 mol^{-1}, compared with overall reaction volumes of between $+19$ and $+26$ cm^3 mol^{-1}. This indicates that electron transfer from Fe to Ru is characterized by an early transition state in terms of volume changes along the reaction coordinate. The overall volume changes could be accounted for in terms of electrostriction effects centered around the ammine ligands on the ruthenium center. A number of possible explanations in terms of electronic and nuclear factors were offered to account for the asymetrical nature of the volume profile (Fig. 18) [109].

One system was investigated where the effect of pressure on the electron-transfer rate constant revealed information on the actual electron-transfer route. We

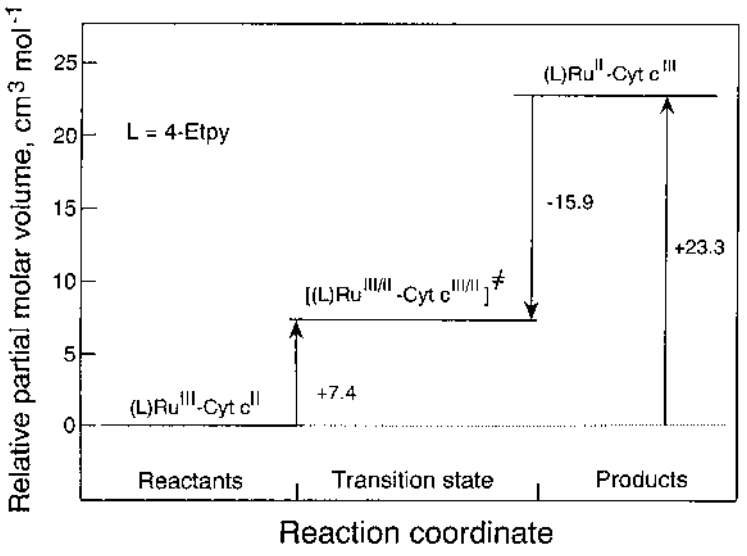

Fig. 18. Volume profile for the reaction [109]

$(NH_3)_4Ru^{III}$(4-Etpy)–cyt $c^{II} \leftrightarrows (NH_3)_4Ru^{II}$(4-Etpy)–cyt c^{III}.

investigated the effect of pressure on distant electronic coupling in $Ru(bpy)_2$(im)-modified His33 and His72 cytochrome *c* derivatives, for which the electron transfer from Fe(II) to Ru(III) is activationless [110]. In the case of the His33-modified system the electron-transfer rate constant exhibited no dependence on pressure within experimental error limits. However, the rate constant for the His72-modified protein increased significantly with increasing pressure, corresponding to a $\Delta V^{\#}$ value of -6 ± 2 cm^3 mol^{-1}. Since this value is exactly opposite to that expected for the reduction of Ru(III), the result was interpreted as an increase in electronic coupling at elevated pressure. The application of moderate pressures will cause a slight compression of the protein that in turn shrinks the through-space gaps that are key units in the electron-tunneling pathway between the heme and His72. A decrease of 0.46 Å in the tunneling path length at a pressure of 150 MPa can account for the observed increase in rate constant. This in turn means that there is an average decrease in the space-gap of 0.1 Å. The absence of an effect for the His33-modified species is understandable since electronic coupling through covalent and hydrogen bonds will be less pressure sensitive than coupling via van der Waals gaps [110].

Very recently, Morishima and co-workers [111] investigated the effect of pressure on electron transfer rates in zinc/ruthenium modified myoglobins. The rate constant for electron transfer from photoexcited ^{3}ZnP* to the $Ru(NH_3)_5^{3+}$ moiety of the protein decreased from 5×10^7 to 55 s^{-1} upon increasing the distance from 9.5 to 19.3 Å when the Ru complex is attached to His70 and His83, respectively. This

decrease in the rate constant was accompanied by an increase in $\Delta V^{\#}$ from $+4$ to $+17$ cm^3 mol^{-1}. Within the context of the results reported above and the volume changes associated with the reduction of the Ru(III) ammine complexes, the gradual increase in $\Delta V^{\#}$ with increasing donor–acceptor distance and with decreasing rate constant could be a clear demonstration of early (for the fast) and late (for the slow reactions) transition states. Volume changes mainly associated with changes in electrostriction on the Ru ammine center will control the solvent reorganization and so account for the early (reactant-like) and late (product-like) transition states.

5. Final remarks

The work presented in this review has illustrated how detailed insight into the reaction mechanisms of coordination complexes can be obtained from a combination of sophisticated kinetic and thermodynamic techniques, studied under a wide range of experimental variables. Such studies can add to our understanding of chemical processes and contribute to our ability to control and design the reactivity of such systems. These aspects therefore complement synthetic/structural studies and highlight the magnificent reaction possibilities as well as reactivities available in coordination chemistry. Our mechanistic insight is restricted by experimental limitations, which calls for kinetic studies to be as detailed as possible, and for suitable theoretical calculations, in order to improve our understanding.

Acknowledgements

Sections of this review were composed by the author while being a Visiting Erskine Fellow at the Department of Chemistry, University of Canterbury, Christchurch, New Zealand. The many stimulating discussions with Don House and his colleagues during that time is very much appreciated. Financial support for our work came from the Deutsche Forschungsgemeinschaft, Bundesministerium für Bildung, Wissenschaft, Forschung und Technologie, Fonds der Chemischen Industrie, Volkswagen-Stiftung, Max-Buchner Forschungsstiftung, German-Israeli Foundation, NATO Scientific Affairs Division, DAAD and the Alexander von Humboldt Stiftung.

References

[1] R. van Eldik (Ed.), Inorganic High Pressure Chemistry: Kinetics and Mechanism, Elsevier, Amsterdam, 1986.
[2] R. van Eldik, J. Jonas (Eds.), High Pressure Chemistry and Biochemistry, Reidel, Dordrecht, 1987.
[3] R. van Eldik, C.D. Hubbard (Eds.), Chemistry under Extreme or Non-Classical Conditions, Wiley, New York, 1997.
[4] R. van Eldik, T. Asano, W.J. le Noble, Chem. Rev. 89 (1989) 549.

[5] R. van Eldik, A.E. Merbach, Comments Inorg. Chem. 12 (1992) 341.
[6] R. van Eldik, in: A.F. Williams, C. Floriani, A.E. Merbach (Eds.), Perspectives in Coordination Chemistry, VHCH, Basel, 1992, p. 52.
[7] G. Stochel, R. van Eldik, Coord. Chem. Rev. 159 (1997) 153.
[8] R. van Eldik, P.C. Ford, Adv. Photochem. 24 (1998) 61.
[9] A. Drljaca, C.D. Hubbard, R. van Eldik, T. Asano, M.V. Basilevsky, W.J. le Noble, Chem. Rev. 98 (1998) 2167.
[10] C.H. Langford, H.B. Gray, Ligand Substitution Processes, W.A. Benjamin, New York, 1965.
[11] R.G. Wilkins, Kinetics and Mechanism of Reactions of Transition Metal Complexes, VCH, Weinheim, 1991.
[12] U. Frey, D.H. Powell, A.E. Merbach, in: J.-J. Delpuech (Ed.), Dynamics of Solutions and Fluid Mixtures by NMR, Wiley, Chichester, 1995, p. 263.
[13] S.F. Lincoln, A.E. Merbach, Adv. Inorg. Chem. 42 (1995) 1.
[14] U. Frey, L. Helm, A.E. Merbach, R. Roulet, in: M. Gielen, R. Willem, B. Wrackmeyer (Eds.), Advanced Applications of NMR to Organometallic Chemistry, Wiley, Chichester, 1996, p. 193.
[15] R. Akesson, L.G.M. Petterson, M. Sandström, P.E.M. Siegbahn, U. Wahlgren, J. Phys. Chem. 96 (1992) 10773.
[16] R. Akesson, L.G.M. Petterson, M. Sandström, P.E.M. Siegbahn, U. Wahlgren, J. Phys. Chem. 97 (1993) 3765.
[17] R. Akesson, L.G.M. Petterson, M. Sandström, U. Wahlgren, J. Am. Chem. Soc. 116 (1994) 8691.
[18] R. Akesson, L.G.M. Petterson, M. Sandström, U. Wahlgren, J. Am. Chem. Soc. 116 (1994) 8705.
[19] F.P. Rotzinger, J. Am. Chem. Soc. 118 (1996) 6760.
[20] F.P. Rotzinger, J. Am. Chem. Soc. 119 (1997) 5230.
[21] R.J. Deeth, L.I. Elding, Inorg. Chem. 35 (1996) 5019.
[22] M. Hartmann, T. Clark, R. van Eldik, J. Am. Chem. Soc. 119 (1997) 5867.
[23] A. Cusanelli, U. Frey, D.T. Ritchens, A.E. Merbach, J. Am. Chem. Soc. 118 (1996) 5265, and literature cited therein.
[24] A. Drljaca, A. Zahl, R. van Eldik, Inorg. Chem. 37 (1998) 3948.
[25] L. Dadci, H. Elias, U. Frey, A. Hörnig, U. Koelle, A.E. Merbach, H. Paulus, J.S. Schneider, Inorg. Chem. 34 (1995) 306.
[26] P. Kofod, P. Harris, S. larsen, Inorg. Chem. 36 (1997) 2258.
[27] C. Eckhard, C. Dücker-Benfer, R. van Eldik, in preparation.
[28] C. Dücker-Benfer, R. Dreos, R. van Eldik, Angew. Chem. Int. Ed. Engl. 34 (1995) 2245.
[29] M. Schmülling, A.D. Ryabov, R. van Eldik, J. Chem. Soc., Dalton Trans. (1994) 1257.
[30] M. Schmülling, D.M. Grove, G. van Koten, R. van Eldik, N. Veldman, A.L. Spek, Organometallics 15 (1996) 1384.
[31] U. Frey, L. Helm, A.E. Merbach, R. Romeo, J. Am. Chem. Soc. 111 (1989) 8161.
[32] R. Romeo, A. Grassi, L.M. Scolaro, Inorg. Chem. 31 (1992) 4383.
[33] G. Laurenczy, I. Rapaport, D. Zbinden, A.E. Merbach, Mag. Res. Chem. 29 (1991) 545.
[34] M. Mizuno, S. Funahashi, N. Nakasuka, M. Tanaka, Inorg. Chem. 30 (1991) 1550.
[35] P.A. Tregloan, S. Seibig, A. Zahl, R. van Eldik, in preparation.
[36] H.C. Bajaj, R. van Eldik, Inorg. Chem. 27 (1988) 4052.
[37] H.C. Bajaj, R. van Eldik, Inorg. Chem. 28 (1989) 1980.
[38] D.H. Powell, P. Furrer, P.-A. Pittet, A.E. Merbach, J. Phys. Chem. 99 (1995) 16622.
[39] D.H. Powell, A.E. Merbach, I. Fabian, S. Schindler, R. van Eldik, Inorg. Chem. 33 (1994) 4468.
[40] A.M. Dittler-Klingemann, C. Orvig, F.E. Hahn, F. Thaler, C.D. Hubbard, R. van Eldik, S. Schindler, I. Fabian, Inorg. Chem. 35 (1996) 7798.
[41] R. van Eldik, H. Cohen, D. Meyerstein, Angew. Chem. Int. Ed. Engl. 30 (1991) 1158.
[42] R. van Eldik, W. Gaede, H. Cohen, D. Meyerstein, Inorg. Chem. 31 (1992) 3695.
[43] R. van Eldik, H. Cohen, D. Meyerstein, Inorg. Chem. 33 (1994) 1566.
[44] T.A. Waldbach, R. van Eldik, P.H. van Rooyen, S. Lotz, Organometallics 16 (1997) 4056.
[45] A.M. Valentine, S.J. Lippard, J. Chem. Soc. Dalton Trans. (1997) 3925.
[46] L. Que, J. Chem. Soc. Dalton Trans. (1997) 3933.
[47] W.B. Tolman, Acc. Chem. Res. 30 (1997) 227.

[48] K.D. Karlin, S. Kaderli, A.D. Zuberbühler, Acc. Chem. Res. 30 (1997) 139.
[49] M. Zhang, R. van Eldik, J.H. Espenson, A. Bakac, Inorg. Chem. 33 (1994) 130.
[50] H.-D. Projahn, C. Dreher, R. van Eldik, J. Am. Chem. Soc. 112 (1990) 17.
[51] D.J. Taube, H.-D. Projahn, R. van Eldik, D. Magde, T.G. Traylor, J. Am. Chem. Soc. 112 (1990) 6880.
[52] H.-D. Projahn, S. Schindler, R. van Eldik, D.G. Fortier, C.R. Andrew, A.G. Sykes, Inorg. Chem. 34 (1995) 5935.
[53] A.L. Feig, M. Becker, S. Schindler, R. van Eldik, S.J. Lippard, Inorg. Chem. 35 (1996) 2590.
[54] V. Zang, R. van Eldik, Inorg. Chem. 29 (1990) 1705.
[55] S. Seibig, R. van Eldik, Inorg. Chem. 36 (1997) 4115.
[56] S. Seibig, R. van Eldik, Eur. J. Inorg. Chem., in press.
[57] M. Becker, S. Schindler, R. van Eldik, Inorg. Chem. 33 (1994) 5370.
[58] S. Goldstein, G. Czapski, R. van Eldik, H. Cohen, D. Meyerstein, J. Phys. Chem. 95 (1991) 1282.
[59] M. Becker, F.W. Heinemann, F. Knoch, W. Donaubauer, G. Liehr, S. Schindler, G. Golub, H. Cohen, D. Meyerstein, Inorg. Chem., submitted for publication.
[60] H.-D. Projahn, R. van Eldik, Inorg. Chem. 30 (1992) 3288.
[61] M. Buchalova, P.R. Warburton, R. van Eldik, D.H. Busch, J. Am. Chem. Soc. 119 (1997) 5867.
[62] M. Buchalova, D.H. Busch, R. van Eldik, Inorg. Chem. 37 (1998) 1116.
[63] D.N. Silverman and S. Lindskog, Acc. Chem. Res. 21 (1988) 30, and the literature survey in Ref. 66.
[64] X. Zhang, R. van Eldik, T. Koike, E. Kimura, Inorg. Chem. 32 (1993) 5749.
[65] X. Zhang, R. van Eldik, Inorg. Chem. 34 (1995) 5606.
[66] X. Zhang, C.D. Hubbard, R. van Eldik, J. Phys. Chem. 100 (1996) 9161.
[67] R. van Eldik, D.A. Palmer, J. Sol. Chem. 11 (1982) 239.
[68] A. Schrodt, A. Neubrandt, R. van Eldik, Inorg. Chem. 36 (1997) 4579.
[69] E. Fujita and R. van Eldik, Inorg. Chem. 37 (1998) 360, and literature cited therein.
[70] C. Geyer, E. Dinjus, S. Schindler, Organometallics 17 (1998) 98.
[71] P. Warneck, Fresenius J. Anal. Chem. 340 (1991) 585.
[72] Ch. Brandt, R. van Eldik, Chem. Rev. 95 (1995) 119.
[73] N. Coichev, R. van Eldik, N. J. Chem. 18 (1994) 123.
[74] J. Kraft, R. van Eldik, Inorg. Chem. 28 (1989) 2297.
[75] E.A. Betterton, J. Atmos. Chem. 17 (1993) 307.
[76] F.F. Prinsloo, Ch. Brandt, V. Lepentsiotis, J.J. Pienaar, R. van Eldik, Inorg. Chem. 36 (1997) 119.
[77] K. Bal Reddy, R. van Eldik, Atmos. Environ. 26 (1992) 661.
[78] Ch. Brandt, I. Fabian, R. van Eldik, Inorg. Chem. 33 (1994) 687.
[79] J. Ziajka, F. Beer, P. Warneck, Atmos. Environ. 28 (1994) 2549.
[80] P. Warneck, J. Ziajka, Ber. Bunsenges. Phys. Chem. 99 (1995) 59.
[81] J. Berglund, S. Fronaeus, L.I. Elding, Inorg. Chem. 32 (1993) 4527.
[82] N. Coichev, R. van Eldik, J. Chem. Educ. 71 (1994) 767.
[83] V. Zang, R. van Eldik, Inorg. Chem. 29 (1990) 4462.
[84] V. Zang, R. van Eldik, J. Chem. Soc., Dalton Trans. (1993) 111.
[85] S.N. Mendiara, E. Ghibaudi, L.J. Perissinotti, A.J. Colussi, J. Phys. Chem. 96 (1992) 8089.
[86] F.F. Prinsloo, J.J. Pienaar, R. van Eldik, H. Gutberlet, J. Chem. Soc., Dalton Trans. (1994) 2373.
[87] F.F. Prinsloo, J.J. Pienaar, R. van Eldik, J. Chem. Soc., Dalton Trans. (1995) 463.
[88] V. Lepentsiotis, F.F. Prinsloo, R. van Eldik, H. Gutberlet, J. Chem. Soc., Dalton Trans. (1996) 2135.
[89] H. Gutberlet, S. Finkler, B. Pätsch, R. van Eldik, H. Gutberlet, VGB Kraftwerktechnik 76 (1996) 139.
[90] F.F. Prinsloo, J.J. Pienaar, R. van Eldik, J. Chem. Soc., Dalton Trans. (1996) 4393.
[91] F.F. Prinsloo, J.J. Pienaar, R. van Eldik, J. Chem. Soc., Dalton Trans. (1997) 1871.
[92] R. van Eldik, in: D. Nocera, J.F. Wishart (Eds.), Photochemisty and Radiation Chemistry: Complementary Methods in the Study of Electron Transfer, Advances in Chemistry Series, vol. 254, American Chemical Society, Washington, 1998.
[93] R. van Eldik, High Press. Res. 6 (1991) 251.

[94] P. Braun, R. van Eldik, J. Chem. Soc., Chem. Commun. (1985) 1349.
[95] I. Krack, R. van Eldik, Inorg. Chem. 25 (1986) 1743.
[96] I. Krack, R. van Eldik, Inorg. Chem. 28 (1989) 851.
[97] I. Krack, R. van Eldik, Inorg. Chem. 29 (1990) 1700.
[98] M. Martinez, M.-A. Pitarque, J. Chem. Soc., Dalton Trans. (1995) 4107.
[99] M. Martinez, M.-A. Pitarque, R. van Eldik, J. Chem. Soc., Dalton Trans. (1996) 2665.
[100] J.F. Wishart, R. van Eldik, J. Sun, C. Su, S.S. Isied, Inorg. Chem. 31 (1992) 3986.
[101] J.J. Sachinidis, R.D. Shalders, P.A. Tregloan, Inorg. Chem. 35 (1996) 2497.
[102] B. Bänsch, M. Meier, M. Martinez, R. van Eldik, C. Su, J. Sun, S.S. Isied, J.F. Wishart, Inorg. Chem. 23 (1994) 4744.
[103] M. Meier, J. Sun, J.F. Wishart, R. van Eldik, Inorg. Chem. 35 (1996) 1564.
[104] J. Sun, J.F. Wishart, R. van Eldik, R.D. Shalders, T.W. Swaddle, J. Am. Chem. Soc. 117 (1995) 2600.
[105] M. Meier, R. van Eldik, Inorg. Chim. Acta 225 (1994) 95.
[106] M. Meier, R. van Eldik, Chem. Eur. J. 3 (1997) 33.
[107] M.T. Cruanes, K.K. Rodgers, S.G. Sligar, J. Am. Chem. Soc. 114 (1992) 9660.
[108] J.I. Sachinidis, R.D. Shalders, P.A. Tregloan, Inorg. Chem. 33 (1994) 6180.
[109] J. Sun, C. Su, M. Meier, S.S. Isied, J.F. Wishart, R. van Eldik, Inorg. Chem., in press.
[110] M. Meier, R. van Eldik, I.-J. Chang, G.A. Mines, D.S. Wuttke, J.R. Winkler, H.B. Gray, J. Am. Chem. Soc. 116 (1994) 1577.
[111] Y. Sugiyama, S. Takahashi, K. Ishimori, I. Morishima, J. Am. Chem. Soc. 119 (1997) 8592.